Published in final edited form as:
ACS Biomater Sci Eng. 2023 January 09; 9(1): 409–426. doi:10.1021/acsbiomaterials.2c00853.

Oxygen Generating Scaffolds for Cardiac Tissue Engineering Applications

Sanika Suvarnapathaki[1,2], **Angelina Nguyen**[2], **Anastasia Goulopoulos**[2], **Gulden Camci-Unal**[2,3]

[1]Biomedical Engineering and Biotechnology Program, University of Massachusetts Lowell, One University Avenue, Lowell, MA, 01854, USA

[2]Department of Chemical Engineering, University of Massachusetts Lowell, One University Avenue, Lowell, MA, 01854, USA

[3]Department of Surgery, University of Massachusetts Medical School, 55 Lake Avenue North, Worcester, MA, 01605, USA

Abstract

Homogeneous vascularization of implanted tissue constructs can extend to 5 weeks, during which cell death can occur due to inadequate availability of oxygen. Researchers are engineering biomaterials that generate and release oxygen in a regulated manner, in an effort to overcome this hurdle. A main limitation with the existing oxygen-generating biomaterials is the uncontrolled release of oxygen, which is ultimately detrimental to the cells. This study demonstrates the incorporation of calcium peroxide (CaO_2) within a hydrophobic polymer, polycaprolactone (PCL), to yield composite scaffolds with controlled oxygen release kinetics sustained over 5 weeks. Oxygen-generating microparticles co-encapsulated with cardiomyocytes in a gelatin-based hydrogel matrix can serve as model systems for cardiac tissue engineering. Specifically, the results reveal that the oxygen-generating microspheres significantly improve the scaffold mechanical strength ranging from 5 ka to 35 kPa, have an average scaffold pore size of 50–100 μm, swelling ratios of 33.3–29.8%, and degradation with 10–49 % remaining mass at the end of 48 hour accelerated enzymatic degradation. The oxygen-generating scaffolds demonstrate improvement in cell viability, proliferation, and metabolic activity compared to the negative control group when cultured under hypoxia. Additionally, the optimized oxygen-generating constructs display no cytotoxicity or apoptosis. These oxygen-generating scaffolds can possibly assist the *in vivo* translation of cardiac tissue constructs.

Graphical Abstract

[†]Correspondence: Gulden_CamciUnal@uml.edu.

Author contributions

G.C.-U conceived the study. G.C.-U. and S.S. designed and planned the experiments. S.S. performed the experiments, analyzed the data, and prepared the final figures. G.C.-U. and S.S. modified the final figures. S.S. and G.C.-U. wrote and revised the manuscript. S. S., A.G., A.N., and G.C.-U. revised, edited, and formatted the manuscript. All authors agree with the submitted version of this manuscript.

Conflict of interest

There are no conflicts to declare.

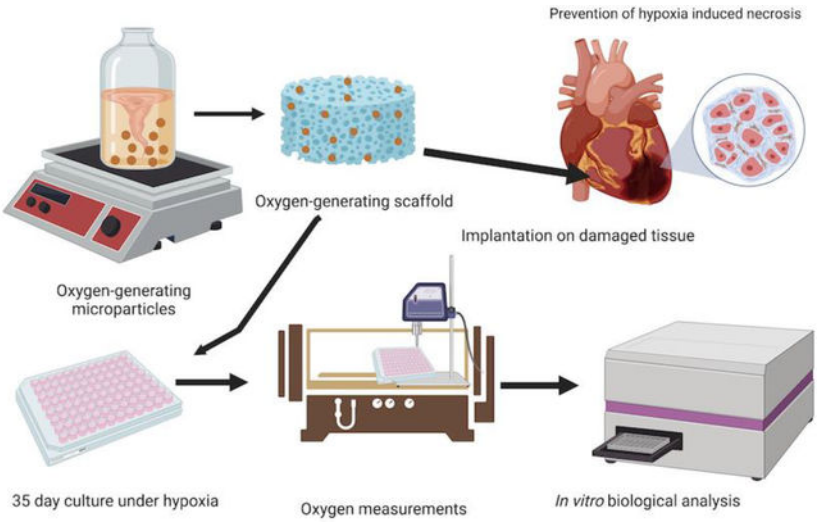

In this work, functional oxygen-generating scaffolds are developed, wherein microparticles containing CaO_2 within PCL are co-encapsulated with cardiac cells in gelatin-based hydrogels. These scaffolds support the viability and metabolic function of cardiac cells under hypoxia for 5 weeks. This unique long-term oxygen generation and release capability of these scaffolds makes them ideal for engineering large scale 3D cardiac tissue constructs.

Keywords

cardiac; tissue-engineering; scaffolds; oxygen-releasing; oxygen-generating

1. Introduction

17.9 million lives are claimed annually by cardiovascular diseases alone, amounting to 31% of deaths worldwide.[1–2] Over 20 million patients suffer from tissue loss associated with cardiovascular ailments. Specifically, chronic heart conditions such as cardiomyopathy, advanced heart failure, arrhythmias, congenital heart disease, coronary artery disease, and heart valve disease significantly contribute to high mortality with scarcely available treatment options.[2–4] For such cardiovascular disorders, tissue engineering approaches can provide an effective solution by reducing the dependency on organ donors.[1]

Current therapies for chronic heart conditions delay the progression of the disease, and commonly involve the use of immunosuppressive drugs following highly invasive surgical procedures. In many cases, the alternative is cardiac transplantation, predominantly dependent

on organ donor availability and compatibility.[5] The long-term clinical success of organ transplantation is dependent on the patient's acceptance of the donor's organ.[6] Therefore, tissue engineering strategies are increasingly being explored and developed in an effort to engineer organ-scale cardiac tissue constructs, decreasing dependency on cardiac transplants. Approaches to engineering cardiac tissue constructs utilize biodegradable polymers to fabricate *in vitro* scaffolds for delivery of cardiac cells for tissue regeneration.[7]

While existing studies have explored a vast array of biomaterials, they are restricted in their functional capabilities to sustain long-term cell viability and metabolic activity.[8–10]

Maintaining high cell viability within artificial constructs proves to be an obstacle for developing 3D organ scale tissue constructs due to diffusion limitations for oxygen and nutrients beyond the 300 μm range.[11–13] Notably, the cardiac tissue is a high oxygen demanding tissue, consuming up to 70 mL O_2/min/100 g oxygen during strenuous activity.[14] Therefore, oxygen availability in cardiac tissue regeneration is vital to facilitating optimum growth and function, and preventing hypoxia-induced necrosis.[15–16] The host's blood is the primary source of oxygen and nutrients to the encapsulated cells in engineered tissue constructs.[11, 16–17] Upon *in vivo* implantation, a tissue-engineered construct can take up to 4 or 5 weeks to effectively integrate with the host's vasculature.[18–21] In recognition of the long integration period, researchers are increasingly seeking to develop approaches to improve vascularization of tissue constructs.[22–24] Nevertheless, attempts solely to improve vascularization do not address the lack of immediate oxygen required for maintaining cell viability and function to ensure the clinical success of the tissue-engineered constructs.[25–28] Consequently, there have been efforts to develop biomaterials with immediate oxygen provision and release within the cellular microenvironment as a potential solution for the high oxygen demand of the surrounding tissues until optimum vascularization can occur.[11, 29] The encapsulation of cells within such oxygen-generating biomaterial scaffolds has garnered a significant scientific incentive.[17, 30–32]

Using oxygen-generating materials enables continuous oxygen availability to encapsulated cells in conventional tissue engineering approaches. In doing so, this strategy permits high cell viability and sustained metabolic activity until complete vascularization can occur.[33] Over the past decade, studies have demonstrated how solid peroxides can be incorporated into 3D scaffolds to generate oxygen by undergoing hydrolytic degradation with the water available in the surroundings or tissue matrices.[11, 31, 34] The recurring obstacle in oxygenation approaches is the burst oxygen release due to rapid hydrolysis of solid peroxides, often yielding reactive oxygen species that could be deleterious to the cells.[3, 35–36] This outburst of oxygen release can be detrimental to cell viability, metabolic activity, and function, all of which are needed for the clinical success of the tissue-engineered constructs.[3, 11] Controlling the hydrolysis reaction rate is a vital element for oxygen-generating materials as it ultimately controls the rate of oxygen release.[37] In an effort to slow down the rate at which water undergoes hydrolytic degradation, utilization of hydrophobic polymers (e.g., poly dimethyl siloxane (PDMS), poly lactic co-glycolic acid (PLGA), and poly vinyl pyrrolidone (PVP)) to encapsulate solid peroxides proves to be an effective approach to regulate the rate of oxygen release. This strategy can prevent the burst release of oxygen from solid peroxides and allow for the prolonged release of oxygen, ultimately supporting cell viability and proliferation under hypoxic conditions until homogeneous vascularization can occur.

Existing approaches have demonstrated limited capability of oxygen-generating biomaterials to release oxygen for only a period of 2–3 weeks.[11] This study demonstrates a novel oxygen-releasing biomaterial for improved viability, growth, and metabolic activity of H9c2 cardiac cells that surpasses the oxygen-releasing capabilities of currently available

oxygen-generating biomaterials. Our biomaterial displayed controlled and sustained oxygen release for up to 4 weeks and lasting oxygen levels up to 5 weeks. Oxygen-generating microspheres were fabricated by encapsulation of calcium peroxide (CaO_2), an oxygen-generating compound, within polycaprolactone (PCL), a hydrophobic polymer, using an emulsification technique. The CaO_2-PCL composite microparticles were co-encapsulated with H9c2 cardiomyocytes within a gelatin methacrylate (GelMA) matrix, which formed the oxygen-generating scaffolds. These scaffolds were then subsequently cultured under hypoxia. Assessment of the cellular response to oxygen-generating scaffolds was performed through various bioassays, after a culture period of 5 weeks under hypoxic and normoxic conditions. Herein, we discuss the physical, chemical, and biological properties of these novel oxygen-generating scaffolds and their implications in supporting cardiac tissue engineering efforts *in vitro*.

2. Materials and methods

2.1. Materials

Polycaprolactone (PCL) pellets (Mw 55,000 GPC) were purchased from Scientific Polymer Products Inc. (Ontario, NY). Calcium peroxide (CaO_2), methacrylic anhydride, and porcine skin gelatin were commercially obtained from Sigma-Aldrich (St. Louis, MO). Dulbecco's Modified Eagle's Medium (DMEM-low glucose), fetal bovine serum (FBS), Dulbecco's phosphate buffered saline (DPBS), trypsin-ethylenediaminetetraacetic acid (EDTA) 0.25%, and penicillin/streptomycin (P/S) were procured from Gibco (Thermo Fisher Scientific, Inc., Waltham, MA). Alamar Blue reagent and lactate dehydrogenase (LDH) activity kit were purchased from Invitrogen (Grand Island, NY). Caspase glo 3/7 assay kit was acquired from Promega (Madison, WI). The photoinitiator 2-hydroxy-1-[4-(hydroxyethoxy) phenyl]-2-methyl-1propanone (Irgacure 2959) was purchased from BASF Corporation (Florham Park, NJ). NeoFox oxygen sensing probe was obtained from Ocean Optics Inc (Dunedin, FL). The hypoxia chamber was obtained from StemCell Technologies (Vancouver, CA). The oxygen sensing probe was NeoFox by Ocean Optics Inc. (Largo, FL). All reagents were used as received without further purification.

2.2. Synthesis of GelMA

The hydrogel precursor comprised of 5% w/v porcine skin gelatin derived gelatin methacrylate (GelMA) and 0.5 % w/v Irgacure 2959 (photoinitiator). The GelMA hydrogel was synthesized using our previously published protocols.[37–39] To synthesize the GelMA hydrogel precursor, 10 g of porcine skin gelatin Type A was dissolved in 100 mL of DPBS under constant magnetic stirring at 50 °C. To the gelatin solution, 8 mL of methacrylic anhydride (MAA) was added dropwise under constant magnetic stirring. The dissolved gelatin mixture with MAA was then allowed to react for 4 hours under constant stirring at 200 rpm at 50 °C. After four hours, the mixture was then diluted with 300 mL of DPBS to stop the methacrylation. Subsequently, the gelatin mixture was dialyzed using nitrocellulose membranes submerged in distilled water for one week under constant magnetic stirring, 180 rpm, at 40 °C. Furthermore, the dialyzed solution was frozen overnight at −80 °C and then lyophilized for one week to obtain the GelMA foam, which was later utilized to make the prepolymer solutions in the photoinitiator solutions. The photoinitiator solutions

were prepared by adding 0.5% w/v Irgacure 2959 in DPBS. Subsequently, the prepolymer solutions were prepared by adding 5% w/v of the GelMA prepolymer foam and dissolving it in the prepared photoinitiator solution. This mixture was then used to fabricate the UV crosslinked oxygen-generating scaffolds.

2.3. Synthesis of oxygen-generating microparticles

Oxygen releasing microparticles were prepared using calcium peroxide (CaO_2), the oxygen-generating compound, encapsulated in a hydrophobic phase made of polycaprolactone (PCL). To synthesize our oxygen-generating microparticles, 13.5% w/v PCL was dissolved in chloroform under constant magnetic stirring at room temperature. CaO_2 was added to the 13.5% w/v PCL solution in varied concentrations of 0, 20, 40, 60, 80 and 100 mg/mL. Successively, upon encapsulation within the GelMA hydrogel matrix, the net CaO_2 concentration amounted to 0, 2.7, 5.4, 8.1, 10.8, and 13.5 mg (Table 1). These scaffold compositions were labeled as OGM0, OGM1, OGM2, OGM3, OGM4, OGM5 respectively. The PCL-CaO_2 solution was magnetically stirred at room temperature to form a viscous complex, serving as the first viscous phase solution. Subsequently, a second aqueous phase solution was prepared by adding 0.5% w/v low molecular weight PVA, which was dissolved in DI water at 80°C. Thus, a two-phase system was formed, wherein the PCL-CaO_2 solution served as the viscous phase, and the PVA solution served as the aqueous phase. Subsequently, the PCL solution was added dropwise to the PVA solution under constant magnetic stirring to synthesize oxygen-generating microparticles. The microparticles were centrifuged at 200 rpm to remove the excess PVA solution and washed three times with chloroform. The microparticles were dried in a vacuum desiccator until the chloroform had evaporated. Subsequently, the PCL-CaO_2 microparticles were homogeneously resuspended within the GelMA prepolymer and UV crosslinked within 96 well plates to form our oxygen-generating scaffolds.

2.4. Engineering oxygen-generating scaffolds

To develop the oxygen-generating scaffolds, 13.5% w/v of oxygen-generating microparticles were homogeneously mixed with 5% w/v GelMA prepolymer by pipetting resuspension. Next, this prepolymer solution containing the oxygen-generating microparticles were pipetted into a 96 well plate with or without cells, followed by UV crosslinking to create the oxygen-generating scaffolds. The scaffolds were crosslinked with UV light (320–500 nm) at an intensity of 4 mW/cm^2 and the cell density across all scaffold groups was maintained a 5×10^6 cells/mL. The scaffolds were cultured with 150 μL of media supplemented with 1 mg/mL catalase under induced hypoxia for five weeks. The oxygen release kinetics were monitored by measuring changes in the partial pressure of oxygen within the supernatant media used to culture these samples. By measuring the daily changes in partial pressure of oxygen over the 35-day culture period, the oxygen-release kinetics were mapped with time for different scaffold compositions. A complete analysis of the scaffolds' physical and biological properties of the scaffolds was performed simultaneously. The mechanical characterization of these oxygen-generating scaffolds was performed and assessed as a bulk material property. To perform mechanical analysis, scaled-up scaffolds were prepared by adding 13.5% w/v oxygen-generating microparticles to 100 μL of GelMA prepolymer, which were then UV crosslinked. The pristine GelMA, OGM0, OGM1, OGM2, OGM3,

OGM4 and OGM5 scaffolds took 20 sec, 30 sec, 60 sec, 70 sec, 90 sec and 140 sec to crosslink respectively. The resulting gels were stored in DPBS and evaluated for swelling, degradation, compression tests, and Scanning Electron Microscopy (SEM) imaging.

2.5. Swelling and Degradation Analysis

The mechanical properties of the oxygen-generating scaffolds were characterized as bulk properties of the material and were therefore performed on larger scaffold volumes. For swelling analysis, the samples were prepared by crosslinking 100 μL of GelMA prepolymer solution with 13.5% w/v oxygen-generating microparticles. Subsequently, the prepolymer solution was UV crosslinked using an Omnicure S2000 (EXFO Photonic Solutions Inc., Ontario, Canada). UV crosslinking time for each gel condition was optimized to be within 20 −140 sec range for the oxygen generating scaffolds. The hydrogels were then submerged in DPBS in petri dishes for 48 hours, wherein the hydrogels reached swelling equilibrium. Swelling analysis was performed in four replicates for each gel composition. Upon reaching swelling equilibrium, the wet weight of each gel was recorded in a pre-weighed empty eppendorf tube, and excess liquid was removed with a Kimwipe. Subsequently, the hydrogel was frozen and lyophilized in eppendorf tubes for 24 hours. After this step, the eppendorf tube was weighed again to obtain the dry weight. Wet weights of the hydrogels were calculated by subtracting the weight of the eppendorf and hydrogel, before lyophilization, from their corresponding empty eppendorf tube. This process was repeated for each replicate to obtain the dry weights of the hydrogels after lyophilization. To determine the swelling ratios, the wet weight of the hydrogels for each condition was divided by the corresponding dry weight, and this ratio was converted into a percentage value.

For degradation analysis, the hydrogel samples were prepared as previously described. Four replicates were performed for each hydrogel composition. After swelling equilibrium, the gels were transferred into pre-weighed eppendorf tubes. These samples were frozen overnight at −80 °C and lyophilized for 24 hours. The initial dry weights were recorded by subtracting the weight of empty eppendorf tubes from the weight of the lyophilized tubes. Subsequently, 1 mL of DPBS was added to the eppendorf tubes to rehydrate the lyophilized gels for 24 hours. After rehydration of the lyophilized gel, the DPBS solution was removed and replaced with 1 mL of 3 U/mL of collagenase type IV in DPBS. The hydrogel samples were incubated at 37 °C on a shaker to facilitate enzymatic degradation. The remaining mass of each hydrogel was measured at different time points (i.e., 3, 6, 12, 18, 24, 36, and 48 hours). The samples were washed with DPBS solution three times to ensure the enzyme solution was completely removed at each time interval. Subsequently, the gels were stored at −80 °C overnight before lyophilization, and the remaining dry weight of the gel sample was recorded after enzymatic degradation. The percent remaining mass after degradation was quantified by the initial and remaining weights of the scaffolds.

2.6. Mechanical testing

For mechanical analysis, the PCL-CaO_2 microparticle reinforced GelMA hydrogels were prepared using the same process as previously described. As mentioned before, the hydrogels were allowed to incubate in DPBS solution for 48 hours, allowing for swelling equilibrium. Prior to performing the compression test, the samples were shaped using an 8

mm biopsy punch, and any residual DPBS solution was removed gently using Kimwipes. Subsequently, the samples were loaded between compression plates and serially exposed to an increasing compressive force. The compression test was performed under certain conditions, which comprised of a preload force of 0.0010 N at an isothermal temperature of 23 °C, force ramp rate of 0.1 N/min, and upper force limit of 2 N. The compressive modulus of each sample was determined by obtaining the slope in the linear region of the stress-strain curve.

2.7. Scanning electron microscopy (SEM) analysis

Using a field emission scanning electron microscope (SEM) (JEOL 5200 SEM), the hydrogel samples were characterized. The SEM images provided morphological characterization of the PCL-CaO_2 microparticle encapsulated oxygen-generating scaffolds. The gel samples were flash-frozen in liquid nitrogen, freeze-dried, mounted on an aluminum stub with double-sided carbon tape, and gold-coated under an argon atmosphere. The sample cross-sections were then hand broken and imaged. Subsequently, the SEM images were acquired to visually observe the porosity and pore size for the pristine GelMA, OGM0, OGM1, OGM2, OGM3, OGM4, and OGM5 scaffolds.

2.8. Oxygen release kinetics

To study the oxygen release kinetics, all scaffolds were cultured under induced hypoxia condition (2% dissolved oxygen) in a StemCell Technologies hypoxia chamber. Under hypoxia, the only available source of oxygen for the cells is the oxygen release from the oxygen-generating microparticles co-encapsulated within the scaffold matrix. We observed lower dissolved oxygen levels throughout the 5-week culture period in samples with cells, under hypoxia conditions, than without cells. Lower dissolved oxygen levels are likely due to cellular consumption of the oxygen released by the oxygen-generating scaffolds.

Furthermore, oxygen levels were observed in the presence and absence of catalase. Catalase is a known enzyme that increase the conversion efficiency of hydrogen peroxide (H_2O_2), a reaction intermediate during the hydrolytic degradation of CaO_2, to water and oxygen.[38–39] Therefore, 1 mg/mL catalase was added to the culture media to investigate significant changes in release kinetics; the resulting oxygen release profile was measured.

2.9. Three-dimensional (3D) cell encapsulation in oxygen-generating hydrogels

For cytocompatibility studies, H9c2 rat cardiomyocytes were encapsulated in the hydrogel precursor solution for pristine GelMA, OGM0, OGM1, OGM2, OGM3, OGM4, and OGM5 at a cell seeding density of 5×10^6 cells/mL. As previously mentioned, the hydrogel precursor solutions were prepared using 5% w/v GelMA for each composition. Subsequently, 13.5% w/v oxygen-generating microparticles was incorporated to the hydrogel precursor. In preparation for 3D encapsulation of the H9c2 rat cardiomyocytes, the cells were trypsinized from the flask, transferred into a conical tube, and centrifuged to obtain a pellet. The cell count was obtained from the cell pellet to determine the appropriate number of cells for homogenous resuspension in the different prepolymer solutions. Subsequently, the cell pellet was resuspended in hydrogel prepolymer solutions containing the oxygen-generating microparticles. Furthermore, the prepolymer solution containing homogeneously dispersed

cells and oxygen-generating microparticles was pipetted into a 96 well plate. This allowed the formation of a stable disc laden with cells and oxygen-generating microspheres within the gel matrix. The hydrogels were then photocrosslinked using the UV light at 4 mW/cm^2 intensity (Figure 1). The cell laden hydrogels with oxygen-generating microparticles were then cultured under hypoxia condition for five weeks. Hydrogel samples were analyzed for their oxygen content, mechanical properties, viability, proliferation, cytotoxicity, and apoptosis to evaluate their effects on the encapsulated cardiomyocytes *in vitro*.

2.10. Cellular response to oxygen-generating scaffolds

To evaluate cellular response to oxygen-generating scaffolds, the cells were resuspended in 5% w/v GelMA prepolymer with 0, 20, 40, 60, 80, and 100 mg/mL CaO_2 in PCL at 13.5 w/v concentration in GelMA. The cell-laden GelMA PCL-CaO_2 scaffolds were cultured in DMEM medium supplemented with 10% v/v fetal bovine serum (FBS) and 5% v/v penicillin/streptomycin. The H9c2 rat cardiomyocyte cultures were maintained in a 37 °C incubator under hypoxia condition (i.e., 2% oxygen (O_2)). The media was changed every two to three days.

The metabolic activity of the cells was measured by performing an Alamar Blue assay using the standard manufacturer's protocol.[40–41] Alamar Blue solution was prepared by combining one-part Alamar Blue dye and nine parts DMEM media. This solution was incubated with the cell laden scaffolds for 4 hours. The fluorometric results were read using a microplate reader in the fluorescence detection mode. The fluorescence values of the resulting supernatant solutions were recorded at 560nm/590nm (Ex/Em). A lactate dehydrogenase (LDH) cytotoxicity assay was performed to evaluate the cytotoxic effects of the oxygen-generating scaffold. LDH assay was performed according to the standard manufacturer's protocol.[41–42] To perform an LDH assay, 50 μL of the sample was pipetted into a 96 well plate and 50 μL of the reaction analyte was added to the solution and allowed to react for 30 minutes, followed by incorporation of a stop solution to the mixture. Absorbance was recorded using a spectrophotometer at 490 nm. This procedure was repeated four times for each scaffold composition.

Cellular apoptosis of H9c2 cardiomyocytes in response to the oxygen-generating scaffold was analyzed by performing a Caspase Glo 3/7 assay using a Caspase Glo 3/7 apoptosis kit (Promega). The reaction substrate was added to the samples in a 1:1 ratio and allowed to react for 45 minutes shielded from light. Following a 45 minutes reaction time, a stop solution was added, and the luminescence of the resulting reacted analyte was recorded, indicative of cellular apoptosis over the culture period.

To analyze the pH change with the incorporation of oxygen-generating microparticles in the scaffold, pH strips were used. To measure the pH of the sample, 20 μL of the supernatant culture media was pipetted on pH strips and observed for resultant color change. The pH measurements were recorded by recoding the color change of the pH strips upon contact with the media that was used to feed the cells encapsulated in different scaffold compositions.

Lastly, the net oxygen consumption per scaffold throughout the 5-week period was assessed by comparing the dissolved oxygen levels in scaffolds with and without cells under hypoxia. Similarly, the oxygen consumption rate of H9c2 cardiomyocytes per scaffold of each day was measured by comparing the dissolved oxygen levels with and without cells under hypoxia. Difference in measured oxygen levels of scaffolds with and without cells were calculated for each day. The net percent dissolved oxygen consumption over 5 weeks in each scaffold was recorded, and the area under the curve was quantified and compared. Moreover, the oxygen consumption rate of the encapsulated H9c2 cardiomyocytes was evaluated within each scaffold composition.

2.11. Statistical analysis

All statistical analyses were performed using GraphPad Prism 6.0 (La Jolla, CA, USA). Results were analyzed by performing a two-way ANOVA. The statistically significant differences were analyzed by performing tukey post hoc tests. In all analyses shown, p-value < 0.05 was considered to be a statistically significant difference. All values are represented as averages ± standard deviation (*$p < 0.05$, **$p < 0.005$, ***$p < 0.005$, and ****$p < 0.0005$).

3. Results

The oxygen-generating scaffolds were developed by adding CaO_2 as an oxygen source at varying concentrations into a PCL solution. PCL functions as a hydrophobic barrier that can regulate how the rate of water, from the surrounding matrix, reacts with the encapsulated CaO_2. This allows the ability to control the rate of hydrolytic degradation of CaO_2 and consequently the oxygen release kinetics of our novel engineered scaffolds. This section summarizes the results from the analyses performed to characterize the physical and biological properties of these oxygen-generating scaffolds and their effects on the encapsulated H9c2 cardiomyocytes.

3.1 Synthesis and characterization of physical properties of oxygen-generating scaffolds

Oxygen-generating microparticles were synthesized utilizing the protocol mentioned in the previous sections with different concentrations of CaO_2 as described in Table 1. After synthesis, the physical appearance, size, and distribution of these oxygen-generating scaffolds were characterized using scanning electron microscopy (SEM). Figure 1 displays the phase contrast image (Figure 1a), SEM image (Figure 1b), and the scaffold cross-sections (Figure 1c). (Figure 1d) demonstrates the size distribution of the oxygen-generating microparticles obtained per batch of the microparticles synthesized. The protocol was optimized to yield composite microparticles with a diameter of 100 μm average size. Subsequently, the microparticles were collected through centrifugation. The magnetic stirrer speed can be optimized to yield 50–250 μm size microparticles, depending on the scalability of the desired application. Using an inverted Zeiss microscope (Maple Grove, MN), we obtained phase-contrast images of the oxygen-generating microparticles after washing them with chloroform and vacuum-drying as displayed in Figure 1a. To synthesize 3D encapsulated oxygen-generating constructs, the oxygen-generating microparticles were weighed out in eppendorf tubes at 13.5 % w/v concentration in the GelMA prepolymer.

Subsequently, this solution was added to the eppendorf, the microparticles were resuspended to ensure homogeneous dispersion, and the resulting solutions were crosslinked with an Omnicure UV lamp S2000 (Ontario, CA). This yielded the 3D encapsulated oxygen-generating hydrogel scaffolds which are displayed in Figure 1. The particle size distribution was obtained by measuring the average diameter of 100 oxygen-generating microparticles for one batch of the PCL-CaO_2 solution, using ImageJ version 1.51. The particle size distribution is provided in Figure 1d.

SEM imaging was performed for the particles using a Field Emission Scanning Electron Microscope (JEOL JSM 7401F) to characterize the physical appearance of the oxygen-generating microparticles. As depicted in Figure 1b. and 1c., the SEM images revealed that the oxygen-generating particles were uniformly embedded within the GelMA matrix. The mechanical properties of the oxygen-generating microparticles were characterized using the DMA compression tests. Our results indicate that the compressive modulus of the scaffolds with oxygen-generating microparticles encapsulated within the GelMA matrix and concentration of CaO_2 encapsulated in the PCL have a linear relationship. As the concentration of CaO_2 encapsulated in the PCL microparticles increases, the compressive modulus of the scaffold also increases. The recorded compressive moduli were 5.0 kPa, 5.9 kPa± 0.9, 10 kPa± 1.6, 15.7 kPa ± 3.8, 20.2 kPa ± 3.5, 25 kPa ± 5.0, 35 kPa ± 5.0 for the pristine GelMA, OGM0, OGM1, OGM2, OGM3, OGM4, and OGM5 scaffolds, respectively (Figure 1e). Furthermore, characterization of the swelling and degradation properties of the oxygen-generating scaffolds was carried out. The scaffolds showed a decrease in swelling ratios as the concentration of CaO_2 in PCL increased. The swelling ratios were 33.3 %, 28.6 %, 28.1 %, 27.9 %, 26.3 %, 22.2 %, and 21.8 % for the pristine GelMA, OGM0, OGM1, OGM2, OGM3, OGM4, and OGM5 scaffolds, respectively (Figure 1f). The degradation results revealed that the scaffolds with the highest CaO_2 concentration in PCL had the highest remaining mass at the end of the degradation period. The percent mass remaining by the end of the degradation experiment was 0 %, 10.2 %, 20.3 %, 35.33 %, 38.2 %, 44.0%, and 49.2 % for the pristine GelMA, OGM0, OGM1, OGM2, OGM3, OGM4, and OGM5 conditions, respectively (Figure 1g).

3.2. Characterization of cellular response

To examine the cellular response of H9c2 cardiomyocytes on the oxygen-generating microparticles, cells were microencapsulated at a cell seeding density of 5×10^6 cells/mL within the hydrogel prepolymer incorporated with 13.5% w/v PCL-CaO_2 microparticle concentration. To examine the oxygen release kinetics, all samples were cultured under hypoxia in a StemCell Technologies Hypoxia Chamber. In this condition, the only source of oxygen for the cells was the co-encapsulated oxygen-generating microparticles. We tested the samples from the pristine GelMA, OGM0, OGM1, OGM2, OGM3, OGM4, and OGM5 scaffold compositions Over 35 days, all scaffold composition were cultured under normoxic or hypoxic conditions, and with or without the catalase enzyme in the culture media.

Dissolved oxygen levels were evaluated during the 35-day culture period. CaO_2 undergoes hydrolytic degradation within the hydrogel matrix and first forms $Ca(OH)_2$ and H_2O_2. H_2O_2 has a short natural shelf life and tends to slowly decompose over time into oxygen and

water[43]. However, with the aid of enzymes such as catalase, H_2O_2 degrades into oxygen and water enzymatically at a faster rate[37]. Therefore, the culture media was supplemented with 1 mg/mL catalase. For *in vivo* applications, the scaffolds can be engineered to contain catalase within the hydrogel to ensure continuous availability of catalase and prevent H_2O_2 build up.

The dissolved oxygen levels were observed to be low for the cells that were cultured under induced hypoxia. Due to the oxygen consumption by the cells, dissolved oxygen levels were lower in the experimental conditions that contained cells compared to that of the conditions that were devoid of cells. The dissolved oxygen levels increased steadily for all scaffold compositions reaching a peak at different time points and subsequently decayed then on, as shown in Figure 2.

For the groups of pristine GelMA, OGM0, OGM1, OGM2, OGM3, OGM4, and OGM5, a peak dissolved oxygen release of 4.9 %, 4.8% between days 1 through 14, 22.0% on day 9, 29.9% on day 16, 35.7% on day 21, 36.2% on day 21, 39.0 on day 21 was observed, respectively, under normoxia condition without catalase in the culture media (Figure 2a). In the presence of catalase under normoxia, peak dissolved oxygen was observed at 8.0% on day 0 through day 14, 7.0% day 0 to day 14, 25.2% on day 11, 31.2% on day 14, 36.8% on day 21, 39.8% on day 21, and 40.4% on day 21 for the previously mentioned scaffold compositions, respectively (Figure 2b).

To study the isolated effects of the oxygen-generating microspheres on the encapsulated cells, the scaffolds were cultured under hypoxia both with and without catalase. The scaffolds cultured under hypoxia without catalase showed peak dissolved oxygen of 5.0% on day 0 with a steady decline to 0.2% on day 35, 5.0% on day 0 with a steady decline to 0.5% on day 35, 16.2% on day 11, 17.2 on day 12, 20.1 on day 22, 24.2% on day 19, and 26.2% on day 20 for the previously mentioned scaffold compositions, respectively (Figure 2c).

The scaffolds cultured under hypoxia with catalase exhibited peak dissolved oxygen level at 5.0% on day 0 with a steady decline to 1.5% on day 35, 5.0% on day 0 with a steady decline to 1.2% on day 35, 14.2% on day 15, 20.2% on day 17, 23.8% on day 17, 29.6% on day 18, and 20.0% on day 18 for the previously mentioned scaffold compositions, respectively (Figure 2d).

The results from our experiments demonstrates that there is a threshold for the dissolved oxygen which is critical for cells to maintain healthy function. This optimal range is expected to vary depending on the cell type, oxygen consumption rate, the cell seeding density, and the volume of the scaffold. These factors could be altered and controlled depending on the specifics of the cardiac tissue to be engineered. We developed highly tunable oxygen-generating scaffolds with varying oxygen release kinetics by regulating the amount of CaO_2 in the oxygen-generating microparticles, concentration of PCL, w/v ratio of CaO_2-PCL microspheres in the hydrogel matrix and seeding density of the cells. The oxygen measurements are highly sensitive to diffusion dynamics of oxygen within the scaffold. To ensure homogeneous diffusion of oxygen throughout the scaffold, the scaffolds were engineered to contain uniform interconnected pores throughout their microstructure. Additionally, a homogeneous distribution of oxygen-generating microparticles was provided

throughout the scaffold thickness. To measure the dissolved oxygen in these scaffolds, an oxygen-sensing probe was used. Since the media diffused throughout the thickness and pores of the scaffold, measuring the changes in the pO_2 of the supernatant media provided a reliable estimate of the net oxygen released by the scaffolds over time.

3.3. Characterization of metabolic activity of the encapsulated H9c2 cardiomyocytes in the oxygen-generating scaffolds

Alamar Blue assay was utilized to assess the effects of the oxygen-generating scaffolds on the metabolic activity of the H9c2 cardiomyocytes. The oxygen-generating scaffolds with microencapsulated H9c2 cardiomyocytes were cultured under normoxia conditions with and without catalase in media. In parallel, oxygen-generating scaffold microencapsulated with H9c2 was cultured under hypoxia condition with and without catalase in media. Alamar Blue assay allowed the assessment of the metabolic activity of the cells by quantification of fluorescence at Ex/Em (560/590). Across all experimental groups, OGM3 scaffold composition demonstrated the highest metabolic activity (Figure 3).

The samples cultured under normoxia without catalase displayed increased metabolic activity up to day 14 and subsequently decreased. As expected, OGM1, OGM2 and OGM3 groups displayed higher metabolic activity compared to the pristine GelMA and OGM0 groups. The OGM4 and OGM5 scaffold composition groups revealed a significant decrease in the cell metabolic activity, indicating that excess oxygen disrupts cell function and growth (Figure 3a).

While the standard normoxic culture condition is 21% partial pressure of oxygen (pO_2) under ambient conditions, the scaffolds under normoxic culture conditions encounter diffusion limitations due to their substantial thickness, scaffold diffusivity which depends on pore size, microparticle loading, and cell density as well as diffusivity of the media. The net pO_2 measured by the oxygen sensing probe is the byproduct of the oxygen present in the media after overcoming the oxygen consumption by the encapsulated cells and diffusivity barriers.

For the scaffolds cultured under normoxic conditions, with catalase in media, OGM3 scaffolds presented the highest metabolic activity across all groups. The metabolic activity showed a similar trend for the scaffolds cultured under normoxia without catalase. The scaffolds under this condition demonstrated an increased metabolic activity up to day 14 and subsequently decreased. Similarly, OGM1, OGM2 and OGM3 scaffolds supported higher metabolic activities at the corresponding time points than the pristine GelMA and OGM0 groups, as expected. The OGM3 scaffold composition displayed the highest metabolic activity amongst the scaffold groups. The OGM4 and OGM5 scaffolds showed a steady decline in the metabolic activity after day 14, indicative of oxidative damage due to excess oxygen (Figure 3b).

Likewise, the OGM3 group showed the highest metabolic activity across all time points in all of the scaffolds cultured under hypoxia without catalase. The OGM4 and OGM5 scaffolds exhibited a decrease in the metabolic activity. Similar to the previous experimental

conditions, the OGM1, OGM2, and OGM3 scaffolds revealed a higher metabolic activity than the pristine GelMA and OGM0 groups (Figure 3c).

For the scaffolds cultured under hypoxia condition with catalase, the highest metabolic activity was observed across all scaffold compositions for the OGM3 condition. As seen in the previous scaffolds, the OGM1, OGM2, and OGM3 scaffolds demonstrated higher metabolic activities than that of the pristine GelMA and OGM0 conditions. As expected, the OGM4 and OGM5 scaffolds caused a decrease in cell metabolic activity even under hypoxia condition (Figure 3d). High metabolic activity in OGM3 and decreased metabolic activity seen in OGM4 and OGM5 conditions indicate that there is an optimum range of dissolved oxygen which supports cell metabolic activity.

It has been reported that the oxygen level to maintain a stable level of ATP increases linearly with the speed a which ATP is consumed.[45] Basic energy requirements for non-beating cardiomyocytes could be met a an extracellular O_2 concentration of less than 0.007 mM[46]. However, this requirement depends largely upon the cell density, metabolic activity, and the physiological state of the cells.[47] The results obtained from our experiments account for optimal dissolved oxygen levels for a constant cell seeding density of 5×10^6 cells/mL. Our *in vitro* scaffolds serve as a baseline model to predict an optimal range for oxygen.

3.4. Cytotoxicity analysis within oxygen-generating scaffolds via lactate dehydrogenase (LDH)

Lactate dehydrogenase (LDH) cytotoxicity assay was performed to analyze the cellular response of microencapsulated H9c2 cardiomyocytes to the oxygen-generating scaffolds LDH is an enzyme released by cells when the cell membrane suffers damage and is indicative of cell death or cytotoxicity.[48] An increase of LDH activity was observed in OGM4 and OGM5 scaffolds, further supporting that a threshold of dissolved oxygen must be met for optimum cell growth and function. The OGM3 scaffolds exhibited the least amount of LDH activity, indicating that OGM3 may be the most suitable scaffold composition for the H9c2 cardiomyocytes.

The LDH activity showed a sharp increase from day 1 to 35 for the pristine GelMA, OGM0, OGM4, and OGM5 scaffolds that were cultured under normoxia condition without catalase. The LDH levels remained constant for the OGM3 scaffolds indicating minimum cytotoxicity in this experimental group. Similarly, an increased LDH activity was seen in the pristine GelMA, OGM0, OGM1, and OGM2 scaffolds. Increased LDH activity is an indicative of increased cytotoxicity, likely due to the absence of sufficient oxygen, within these scaffolds. Similarly, an increased LDH activity was observed in OGM4 and OGM5 scaffolds, indicating increased cytotoxicity due to excess amount of oxygen (Figure 4a).

In comparison, scaffolds cultured under normoxia with catalase revealed higher cytotoxicity than the without catalase group. This could be attributed to the presence of excess dissolved oxygen in the culture media. As foreseen, the OGM3 scaffolds elicited the least amount of increase in the LDH activity. The pristine GelMA, OGM0, OGM1, OGM2 groups triggered a steady increase in LDH activities over the 35 day culture period. The OGM4 and OGM5 groups revealed a sharp increase in the LDH activity, indicative of cell damage (Figure 4b).

For the scaffolds cultured under hypoxia conditions, without catalase, the OGM3 group revealed the least increase in the LDH activity, remaining constant throughout the culture period. The LDH activity showed a significant increase for the pristine GelMA, OGM0, OGM1, and OGM2 scaffolds, due to the lack of sufficient oxygen. Similarly, the OGM4 and OGM5 conditions showed a sharp increase in the LDH activity, likely due to excess oxygen release resulting in oxidative damage (Figure 4c).

The scaffolds cultured under hypoxia condition with catalase in the media, presented the slightest increase in the LDH activity across all experimental conditions. The addition of catalase to the culture medium under hypoxia increases the conversion efficiency of H_2O_2 to oxygen and water. This prevents excessive buildup of extracellular H_2O_2 while increasing the net oxygen release. There is a range of oxygen concentrations which proves to be beneficial to cellular metabolic health. However, excessive oxygen a rapid rates can be detrimental to cell health[47, 49]. Therefore, in the presence of catalase, we see higher LDH levels for the OGM4 and OGM5 groups due to excess oxygen formation in the culture media.

As observed in the previous results, the OGM3 group caused no significant increase in the LDH activity. Similarly, the pristine GelMA, OGM0, OGM1, and OGM2 demonstrated a steady increase in the LDH activity by day 35. The OGM4 and OGM5 exhibited a significant increase in the LDH activity from day 1 through day 35. LDH is an enzyme that is released when there is a damage to the cell membrane as experienced during cytotoxicity.[44,49] Higher levels of LDH are indicative of higher amount of damage to the cell membrane which occurs when the cells experience cytotoxicity. Therefore, decreased LDH levels indicated by low absorbance readings are indicate of lower cytotoxicity. When cells are metabolically healthy, the LDH activity is expected to be low, which is shown by the lowest LDH levels for the OGM3 scaffolds corresponding to highest metabolic activity, as expected.

3.5. Characterization of apoptosis within oxygen-generating scaffolds

Further evaluation of the cellular response of encapsulated H9c2 cardiomyocytes towards the oxygen-generating scaffolds was done by performing Caspase Glo 3/7 assays. Caspase Glo 3/7 assay emits a luminescence proportional to the amount of apoptosis, allowing for quantification. The cellular metabolic activity despite their high oxygen content, indicating excessive oxygen concentrations decrease the cellular metabolic activity.

The results revealed that the scaffolds cultured under normoxia without catalase, indicated a slight increase in apoptosis. The pristine GelMA, OGM0, OGM1, OGM4, and OGM5 groups demonstrated a significant increase in apoptosis from day 1 to day 35. Comparatively, the OGM2 and OGM3 scaffolds showed no significant increase in apoptosis. This result can be attributed to the low oxygen levels observed in the pristine GelMA, OGM0, and OGM1 scaffolds and the contrastingly high dissolved oxygen levels recorded in the media used to culture the OGM4 and OGM5 scaffolds which could be a cause for oxidative damage to the cardiomyocytes (Figure 5a).

The results for the scaffolds cultured under normoxia condition with catalase, presented a minor increase in apoptosis for the pristine GelMA, OGM0, OGM1, OGM2, and OGM3 groups between days 1 to 35. Similarly, this finding was significantly lower compared to the apoptosis observed for the OGM4 and OGM5 groups (Figure 5b). The scaffolds cultured under hypoxia condition without catalase elicited a significant increase in apoptosis from day 1 to 35. Specifically, the pristine GelMA, OGM0, OGM1, and OGM2 had insufficient oxygen supply under hypoxia. However, this increase in apoptosis was lower than that of the OGM4 and OGM5 groups, which was due to unnaturally high dissolved oxygen levels recorded within the media used to culture these scaffold groups. The scaffolds cultured under hypoxia with catalase displayed improved apoptosis response in the presence of catalase. The OGM3 group had the lowest increase in apoptosis from day 1 to 35. The pristine GelMA, OGM0, OGM1, and OGM2 scaffolds revealed a significant increase in cellular apoptosis during the entire culture period.

Nevertheless, it was still significantly lower compared to the apoptosis response from the OGM4 and OGM5 groups, which showed the highest cellular apoptosis across all time intervals.

3.6. Characterization of change in pH within oxygen-generating scaffolds

The pH of the media was monitored across all groups using pH strips. 20 μL of supernatant media was added on the surface of the pH strips and the color change was compared against a calibrated pH indicator. It was observed that for the scaffolds cultured under normoxia without catalase, the pH remained constant between 8 to 8.5 for the pristine GelMA and negative control group scaffolds with respect to the scaffolds with higher concentrations of CaO_2. There was no significant increase in the pH values observed across all groups.

A pH of 9 was observed across all scaffold groups that were cultured under normoxia with catalase in the culture media. Simultaneously, the scaffolds cultured under hypoxia without catalase, presented a pH values of 8, 8, 8.5, 8.5. 8.5, 8.5, 8.5 for thepristine GelMA, OGM0, OGM1, OGM2, OGM3, OGM4, and OGM5 groups, respectively.

Similarly, the scaffolds cultured under hypoxia condition with catalase, exhibited pH values of 8.5–9 across all scaffold groups. Collectively, the results revealed no significant change in the pH of the supernatant media in the presence of the oxygen-generating microspheres over the 35-day culture period. Therefore, it was evident that these scaffolds did not elicit pH-induced cell damage.

3.7. Evaluation of the oxygen consumption behavior and oxygen consumption rate of the encapsulated cardiomyocytes

The rate of oxygen consumption by the encapsulated H9c2 cardiomyocytes was evaluated by measuring the dissolved oxygen content within the supernatant media used to culture the cell laden scaffolds over the 35-day culture period. The daily peak dissolved oxygen measurements were recorded within the supernatant media used to culture scaffolds laden with cells and scaffolds devoid of cells. By calculating the difference between the oxygen readings recorded for scaffolds without cells and scaffolds with cells, the oxygen

consumption capacity and rate of the cells were quantified. The calculated net oxygen consumption trend was plotted in Figure 6a.

The oxygen consumption kinetics were depicted and compared by evaluating the area under the curve for the oxygen measurements recorded for each scaffold composition (Figure 6b). The comparative analyses revealed that the OGM3 scaffolds showed the highest oxygen consumption capacity under hypoxia. Furthermore, the oxygen consumption profiles were consistent with the metabolic activity results. The OGM3 scaffolds showed the highest metabolic activity which correspondingly showed highest net oxygen consumption. Additionally, % oxygen consumed per day was calculated for each scaffold composition (Figure 6c). The average oxygen consumption rate was 1.4%, 2.4%, 3.6%, 4.3%, 3.8%, and 3.9% per scaffold each day for OGM0, OGM1, OGM2, OGM3, OGM4, and OGM5 scaffolds, respectively (Figure 6d).

The statistical analysis of the data revealed that the OGM3 scaffolds have a significantly higher oxygen consumption rate as compared to the other scaffold groups. OGM2 and OGM4 showed comparable average oxygen consumption rates. OGM0 and OGM1 understandably had the lowest consumption rates considering their lowest oxygen content which was insufficient to alleviate the hypoxia-induced cell death as corroborated by the Alamar Blue, LDH, and caspase assays.

4. Discussion

Oxygen-generating biomaterials have promising potential to facilitate the development of clinically relevant 3D cardiac tissue constructs. However, various challenges remain to be Addressed to engineer oxygen-generating scaffolds that can provide controlled and sustained oxygen release over extended periods of time.[32] The problems associated with uncontrolled burst release of oxygen, poor control over oxygen release kinetics, and low oxygen release capacity, affected the efficiency of these materials.[50–51] In this study, we developed novel oxygen-generating scaffolds that can release oxygen in a controlled and sustained manner over a period of 5 weeks. To engineer these scaffolds, oxygen-generating microspheres were developed using an emulsification technique. Calcium peroxide (CaO_2) was encapsulated within polycaprolactone (PCL), then co-encapsulated with H9c2 cardiomyocytes in a gelatin methacrylate (GelMA) matrix to form the oxygen-generating scaffolds.

The concentrations of calcium peroxide were chosen and optimized with respect to the crosslinking limit of the scaffold. It is important to crosslink the scaffolds rapidly and minimize the UV exposure times to avoid potential damage to the cells. Therefore, the highest amount of CaO_2 loading was chosen and optimized based on the UV exposure time necessary to fully crosslink these scaffolds and subsequently tested for biocompatibility *in vitro*. Additional factors such as the oxygen release potential of these scaffolds was also assessed by monitoring the oxygen release rate for each CaO_2 concentration, starting with the highest concentration. The concentration which provided the most optimal UV crosslinking time, cytocompatibility response, and controlled and sustained oxygen release up to 5 weeks, was chosen as the highest CaO_2 loading concentration. The lower

concentrations were spaced out evenly to better understand the effects of lower CaO_2 concentrations on release kinetics, physical properties, and cellular response over time.

Various characterization techniques were utilized to understand the physical and mechanical properties of these composite scaffolds. The results confirmed that the physical properties (i.e., compressive modulus, swelling, and degradation) of our novel oxygen-generating scaffolds can be altered by varying the CaO_2 concentration in PCL. This allows the development of highly tunable scaffolds which could enable the advancement of cardiac tissue constructs of varying sizes and dimensions.

Swelling analysis revealed an inverse relationship between the swelling ratio and oxygen-generating microparticle content in the hydrogel matrix. This swelling behavior was as attributed to the fact that increasing the CaO_2 concentration within the composite scaffolds led to an increase in the non-hydrophilic content in the constructs, ultimately resulting in the reduction of the hydrophilic content. Consequently, the scaffolds held lower amounts of water with lower swelling ratios.

The degradation study was performed under accelerated enzymatic conditions, explicitly targeting the degradation of the gelatin component of the oxygen-generating scaffolds using collagenase Type IV. Hence, the scaffolds with higher calcium peroxide content had a higher percent remaining mass after accelerated degradation. Utilizing collagenase for accelerated degradation allowed the oxygen-generating PCL-CaO_2 microparticles to remain intact within the scaffold. Therefore, scaffolds with increased microparticle content presented less degradation. However, in *in vivo* applications, it is expected that both the gelatin component and the oxygen-generating microparticles would degrade. The degradation rate can be easily regulated by modifying the concentration of GelMA, the amount of microparticles, gel volume, and crosslinking density. Moreover, these PCL-CaO_2 microparticle systems can also act as controlled release systems allowing for modifications and controlled release of degradation enzymes, growth factors, and biomolecules to facilitate tissue development. This feature can be used effectively to further control the degradation rate of the scaffolds.

Furthermore, the mechanical properties of the oxygen-generating scaffolds were analyzed by conducting a dynamic compression test. The compression test revealed that the addition of PCL-CaO_2 microparticles mechanically reinforced the scaffolds.

While the w/v concentration of the oxygen-generating microparticles in each scaffold composition was maintained constant, increasing concentrations of CaO_2 led to an increasing trend in the compressive strength. The addition of higher concentrations of CaO_2 mechanically reinforced the scaffolds and consequently increased the compressive strength of the scaffolds. Therefore, the compressive strength can be easily regulated depending on the mechanical properties of the target tissue.

The SEM imaging of the scaffolds revealed the porous structure and distribution of the oxygen-generating microparticles within the scaffolds. A homogeneous distribution of interconnected pores were observed in the scaffolds which can allow improved oxygen and nutrient diffusion and cellular interactions.[52] The healthy cellular metabolic activity observed from Alamar Blue results validated this observation. The interconnected

pores also closely mimic the biomechanical cues experienced by the cells within their microenvironment. The porous structures also enable better diffusion of the generated oxygen within the scaffolds while allowing for enhanced cell-cell interaction.

After evaluation of the physical properties of the oxygen-generating scaffolds, the oxygen release kinetics of the scaffolds were characterized by measuring the dissolved oxygen levels under hypoxia and normoxia in the presence and absence of cells. The dissolved oxygen levels revealed that the peak percentage dissolved oxygen levels increased proportionally as the concentrations of the CaO_2 in the scaffolds augmented. The oxygen release in the scaffolds, occurs as a by product of the hydrolytic degradation of CaO_2.

$$(\text{Calcium peroxide})\ CaO_2(s) + 2H_2O \rightarrow Ca(OH)_2(s) + H_2O_2$$

$$2H_2O_2 \rightarrow O_2 + 2H_2O$$

11

Consequently, an increase in the CaO_2 loading resulted in an increased oxygen generation. The PCL component being a hydrophobic co-polymer, slowed down the rate at which the water from the surrounding GelMA hydrogel could diffuse and degrade the CaO_2. Therefore, the addition of PCL, regulated the rate of hydrolysis of CaO_2, which thereby led to controlled release of oxygen. Additionally, the culture media was supplemented with catalase at a concentration of 1 mg/mL which further ensured conversion of the intermediate H_2O_2 to oxygen while avoiding any H_2O_2 related cellular damage.

The oxygen measurement results also revealed that as the concentration of CaO_2 in the oxygen-generating microparticles increased, the corresponding peak dissolved oxygen in the media increased. Similarly, the peak oxygen release was observed at later time points within the 35-day culture period for the conditions with higher CaO_2 loading. This was indicative of prolonged release potential with slower release rates. For instance, for the OGM3, OGM4, and OGM5 groups, peak release was attained at later time points when compared to the OGM0, OGM1, and OGM2 scaffolds. Dissolved oxygen levels were recorded from the supernatant media which was used to culture the oxygen-generating scaffolds under normoxia or hypoxia, with or without catalase. The comparison between different scaffold conditions demonstrates a highly tunable oxygen release can be achieved using our novel oxygen-generating scaffolds.

Additionally, the biological compatibility of the oxygen-generating scaffolds was evaluated to understand their ability to support the viability and proliferation of the cardiac cells exposed to the oxygen-generating scaffolds. To analyze the biocompatibility, H9c2 cardiomyocytes were microencapsulated at a cell density of 5 million cells/mL within the oxygen-generating scaffolds. Subsequently, a series of biological assays (i.e., Alamar Blue, LDH, and Caspase Glo 3/7) were performed to assess the cardiac cell response to the oxygen-generating scaffolds under hypoxia and normoxia. These assays collectively revealed that the OGM3 scaffolds elicited the most favorable cellular metabolic activity, and

reduced cytotoxicity and apoptosis. In comparison, the OGM4 and OGM5 scaffolds induced the opposite effect for the 3D encapsulated cardiomyocytes. This result indicates that there is an optimum range of oxygen-generating microparticle compositions that are most favorable to support cardiomyocytes. If this range is exceeded, the amount of released oxygen can be detrimental to cardiomyocytes. This range was also heavily dependent on the amount of CaO_2 loaded within the PCL, provided the PCL concentration was kept constant. We would expect that changes in the PCL concentration, w/v ratio of the microparticles within GelMA, cell seeding density, and the w/v concentration of GelMA itself would also act as variables which can significantly be tuned to obtain the desired oxygen-release kinetics.

Furthermore, we investigated whether the presence of catalase in the media would significantly influence the release kinetics of oxygen. The experiments were performed by incorporating 1 mg/mL catalase in the media. Catalase is an enzyme that is produced by the liver and increases the conversion efficiency of hydrogen peroxide to water and oxygen.[11, 54–55] Therefore, the addition of catalase is expected to increase the release potential and accelerate the oxygen release kinetics. Our results indicated that the presence of 1 mg/mL catalase in media improved the conversion efficiency of the hydrogen peroxide to oxygen and water, ultimately displaying higher oxygen levels compared to the absence of catalase in the media. Additionally, the presence of catalase for the cell-laden oxygen-generating scaffolds resulted in lower dissolved oxygen levels, as the cells consume the released oxygen over time. The addition of catalase also is known to prevent the build up of H_2O_2 and any reactive oxygen species which can be harmful to the cells. This could offer additional advantages to using catalase in the oxygen-generating scaffold cultures.[55–56]

Finally, the pH of the supernatant media was measured across all scaffold compositions showed no significant increase over the 35-day culture period. This result demonstrated no drastic pH changes occurred in the media due to reaction intermediates formed during the hydrolytic degradation of CaO_2. Furthermore, our Alamar Blue, LDH, and apoptosis assays demonstrated that CaO_2 is biocompatible and not detrimental to cells during prolonged exposure under hypoxia. Similar results about the biocompatibility and biodegradation behavior of CaO_2 were found in the previous literature studies.[57–60]

The ability of our scaffolds to provide sustained oxygen release over 5 weeks, is a remarkable improvement over existing oxygen-generating biomaterials. Our novel scaffolds overcome the oxygen diffusion limitations which can significantly enhance the long-term viability and *in vivo* success of organ scale tissue constructs. When paired with efforts to improve vascularization, these oxygen-generating materials could serve as a critical link to bringing organ scale cardiac tissue constructs closer to translation.

5. Conclusion

In this work, novel oxygen-generating scaffolds with unique sustained oxygen release capabilities were developed. The interaction of these scaffolds with cardiac muscle cells as a tissue engineering model was thoroughly investigated. Overall, the results revealed that the PCL-CaO_2 composite oxygen-generating microparticles, encapsulated within GelMA hydrogels with cardiac cells, helped to improve cell proliferation, and metabolic

activity under hypoxic conditions. The oxygen-generating scaffolds exhibited high degree of tunability in their physical properties such as swelling behavior, degradation rate, porosity, and mechanical strength which helped the development of compatible scaffolds. Furthermore, *in vitro* assessment of these scaffolds proved that these oxygen- generating scaffolds exhibit biodegradability and cytocompatibility. Our novel oxygen-generating scaffold provided sufficient oxygen generation which was regulated over 5 weeks. In addition to the oxygen release, the scaffolds were able to provide prolonged dissolved oxygen levels under hypoxic conditions over 5 weeks. Overall, the results revealed that the OGM3 scaffolds provided the most favorable cellular response when cultured under hypoxia condition with catalase in media. This release potential depended largely on the CaO_2 loading, and presence of catalase in the media, since other parameters such as PCL concentration, GelMA concentration, and cell density were maintained constant throughout all the release kinetics, metabolic activity, and oxygen consumption kinetics collectively revealed a range of CaO_2 concentrations within PCL that offer the most favorable cellular response. Overall, the OGM3 scaffold composition demonstrated the most favorable cellular response under all culture conditions. Conversely, despite providing high dissolved oxygen content to the encapsulated cells, the OGM4 and OGM5 scaffolds elicited increased cytotoxicity and apoptosis, which was indicative that excess oxygen was detrimental to normal cell function. This finding signifies that there is a threshold for the dissolved oxygen which is critical for cells to maintain healthy function. This optimal range is expected to vary depending on the cell type, oxygen consumption rate, the cell seeding density, and the volume of the scaffold. These factors could be altered and controlled depending on the specifics of the cardiac tissue to be engineered. We developed highly tunable oxygen-generating scaffolds with varying oxygen release kinetics by regulating the amount of CaO_2 in the oxygen-generating microparticles, concentration of PCL, w/v ratio of CaO_2-PCL microspheres in the hydrogel matrix, and seeding density of the cells. These oxygen-generating scaffolds can prevent burst release of oxygen, help cells overcome hypoxia-induced necrosis, and allow integration with the cellular microenvironment. Furthermore, the effect of CaO_2 on the pH was examined and revealed that the extracellular pH is not significantly impacted. The scaffolds showed compatible oxygen release capabilities sufficient for satisfying the oxygen demand of the encapsulated H9c2 cardiomyocytes. consistent with high net oxygen release capacity and net oxygen consumption rate recorded. This study successfully demonstrated the cytocompatibility and biodegradability of the oxygen-generating scaffolds *in vitro* for the H9c2 cardiomyocytes. Furthermore, our novel oxygen-generating biomaterials can serve as an excellent platform to assess their use with different cell types in the future. These scaffolds can be useful for a range of metabolically active and high oxygen demanding tissues. Utilizing oxygen-generating scaffolds could ultimately pave way for successful *in vivo* translation of cardiac tissue constructs.

Acknowledgements

This research was partly funded by the UMass Lowell faculty startup funds and a Transformational Project Award from the American Heart Association (AHA) (19TPA34910111).

References

1. Transplantation, U. S. G. I. o. O. D. a. Organ Donation Statistics. https://www.organdonor.gov/statistics-stories/statistics.html (accessed July).
2. Mc Namara K; Alzubaidi H; Jackson JK, Cardiovascular disease as a leading cause of death: how are pharmacists getting involved? Integr Pharm Res Pract 2019, 8, 1–11. [PubMed: 30788283]
3. Alemdar N; Leijten J; Camci-Unal G; Hjortnaes J; Ribas J; Paul A; Mostafalu P; Gaharwar AK; Qiu Y; Sonkusale S; Liao R; Khademhosseini A, Oxygen-Generating Photo-Cross-Linkable Hydrogels Support Cardiac Progenitor Cell Survival by Reducing Hypoxia-Induced Necrosis. ACS Biomaterials Science & Engineering 2017, 3 (9), 1964–1971. [PubMed: 33440552]
4. Mavroudis C; Dearani JA, Anatomic Variation for Cardiac Transplantation in Adults with Congenital Heart Disease. In Atlas of Adult Congenital Heart Surgery, Springer: 2020; pp 413–422.
5. Messner F; Guo Y; Etra JW; Brandacher G, Emerging technologies in organ preservation, tissue engineering and regenerative medicine: a blessing or curse for transplantation? Transpl Int 2019, 32 (7), 673–685. [PubMed: 30920056]
6. Heidt S; Haasnoot GW; Witvliet MD; van der Linden-van Oevelen MJH; Kamburova EG; Wisse BW; Joosten I; Allebes WA; van der Meer A; Hilbrands LB; Baas MC; Spierings E; Hack CE; van Reekum FE; van Zuilen AD; Verhaar MC; Bots ML; Drop ACAD; Plaisier L; Seelen MAJ; Sanders J-S; Hepkema BG; Lambeck AJA; Bungener LB; Roozendaal C; Tilanus MGJ; Voorter CE; Wieten L; van Duijnhoven EM; Gelens MACJ; Christiaans MHL; van Ittersum FJ; Nurmohamed SA; Lardy NM; Swelsen W; van der Pant KAMI; van der Weerd NC; ten Berge IJM; Bemelman FJ; Hoitsma A; van der Boog PJM; de Fijter JW; Betjes MGH; Otten HG; Roelen DL; Claas FHJ, Allocation to highly sensitized patients based on acceptable mismatches results in low rejection rates comparable to nonsensitized patients. American Journal of Transplantation 2019, 19 (10), 2926–2933. [PubMed: 31155833]
7. Iqbal N; Khan AS; Asif A; Yar M; Haycock JW; Rehman IU, Recent concepts in biodegradable polymers for tissue engineering paradigms: a critical review. International Materials Reviews 2019, 64 (2), 91–126.
8. Roshanbinfar K; Mohammadi Z; Mesgar AS-M; Dehghan MM; Oommen OP; Hilborn J; Engel FB, Carbon nanotube doped pericardial matrix derived electroconductive biohybrid hydrogel for cardiac tissue engineering. Biomaterials science 2019, 7 (9), 3906–3917. [PubMed: 31322163]
9. Zargar SM; Mehdikhani M; Rafienia M, Reduced graphene oxide–reinforced gellan gum thermoresponsive hydrogels as a myocardial tissue engineering scaffold. Journal of Bioactive and Compatible Polymers 2019, 34 (4–5), 331–345.
10. Zhang F; Zhang N; Meng H-X; Liu H-X; Lu Y-Q; Liu C-M; Zhang Z-M; Qu K-Y; Huang N-P, Easy applied gelatin-based hydrogel system for long-term functional cardiomyocyte culture and myocardium formation. ACS Biomaterials Science & Engineering 2019, 5 (6), 3022–3031. [PubMed: 33405656]
11. Suvarnapathaki S; Wu X; Lantigua D; Nguyen MA; Camci-Unal G, Breathing life into engineered tissues using oxygen-releasing biomaterials. NPG Asia Materials 2019, 11 (1), 65.
12. Seiler TG; Komninou MA; Nambiar MH; Schuerch K; Frueh BE; Büchler P, Oxygen Kinetics During Corneal Cross-linking With and Without Supplementary Oxygen. American journal of ophthalmology 2021, 223, 368–376. [PubMed: 33227242]
13. Afshari E; Khodabakhsh S; Jahantigh N; Toghyani S, Performance assessment of gas crossover phenomenon and water transport mechanism in high pressure PEM electrolyzer. International Journal of Hydrogen Energy 2021, 46 (19), 11029–11040.
14. Giordano FJ, Oxygen, oxidative stress, hypoxia, and heart failure. The Journal of clinical investigation 2005, 115 (3), 500–508. [PubMed: 15765131]
15. Chandy T, 12 - Biocompatibility of materials and its relevance to drug delivery and tissue engineering. In Biointegration of Medical Implant Materials (Second Edition), Sharma CP, Ed. Woodhead Publishing: 2020; pp 297–331.
16. Suvarnapathaki S; Nguyen MA; Goulopoulos AA; Lantigua D; Camci-Unal G, Engineering calcium peroxide based oxygen generating scaffolds for tissue survival. Biomaterials Science 2021, 9 (7), 2519–2532. [PubMed: 33565527]

17. Rademakers T; Horvath JM; van Blitterswijk CA; LaPointe VLS, Oxygen and nutrient delivery in tissue engineering: Approaches to graft vascularization. J Tissue Eng Regen Med 2019, 13 (10), 1815–1829. [PubMed: 31310055]
18. Camci-Unal G; Alemdar N; Annabi N; Khademhosseini A, Oxygen Releasing Biomaterials for Tissue Engineering. Polym Int 2013, 62 (6), 843–848. [PubMed: 23853426]
19. Fleischer S; Tavakol DN; Vunjak-Novakovic G, From arteries to capillaries: approaches to engineering human vasculature. Advanced Functional Materials 2020, 30 (37), 1910811. [PubMed: 33708027]
20. Oliveira H; Médina C; Labrunie G; Dusserre N; Catros S; Magnan L; Handschin C; Stachowicz M; Fricain J; L'Heureux N, Cell-assembled extracellular matrix (CAM): a human biopaper for the biofabrication of pre-vascularized tissues able to connect to the host circulation *in vivo*. Biofabrication 2021, 14 (1), 015005.
21. Cho WW; Kim BS; Ahn M; Ryu YH; Ha DH; Kong JS; Rhie JW; Cho DW, Flexible Adipose-Vascular Tissue Assembly Using Combinational 3D Printing for Volume-Stable Soft Tissue Reconstruction. Advanced Healthcare Materials 2021, 10 (6), 2001693.
22. Bannerman AD; Ze Lu RX; Korolj A; Kim LH; Radisic M, The use of microfabrication technology to address the challenges of building physiologically relevant vasculature. Current Opinion in Biomedical Engineering 2018, 6, 8–16.
23. Tan SY; Leung Z; Wu AR, Recreating Physiological Environments In Vitro: Design Rules for Microfluidic-Based Vascularized Tissue Constructs. Small 2020, 16 (9), 1905055.
24. Morrison E; Suvarnapathaki S; Blake L; Camci-Unal G, Unconventional Biomaterials for Cardiovascular Tissue Engineering. Current Opinion in Biomedical Engineering 2021, 100263.
25. Khakpoor N; Mostafavi E; Mahinpey N; De la Hoz Siegler H, Oxygen transport capacity and kinetic study of ilmenite ores for methane chemical-looping combustion. Energy 2019, 169, 329–337.
26. Pavlacky J; Polak J, Technical feasibility and physiological relevance of hypoxic cell culture models. Frontiers in endocrinology 2020, 11, 57. [PubMed: 32153502]
27. Weits DA; van Dongen JT; Licausi F, Molecular oxygen as a signaling component in plant development. New Phytologist 2021, 229 (1), 24–35. [PubMed: 31943217]
28. Richards DJ; Li Y; Kerr CM; Yao J; Beeson GC; Coyle RC; Chen X; Jia J; Damon B; Wilson R, Human cardiac organoids for the modelling of myocardial infarction and drug cardiotoxicity. Nature biomedical engineering 2020, 4 (4), 446–462.
29. Soltani M; Maleki MA; Kaboodrangi AH; Mosadegh B, Optimization of oxygen transport within a tissue engineered vascular graft model using embedded micro-channels inspired by vasa vasorum. Chemical Engineering Science 2018, 184, 1–13.
30. Gholipourmalekabadi M; Zhao S; Harrison BS; Mozafari M; Seifalian AM, Oxygen-Generating Biomaterials: A New, Viable Paradigm for Tissue Engineering? Trends in Biotechnology 2016, 34 (12), 1010–1021. [PubMed: 27325423]
31. Lu Z; Jiang X; Chen M; Feng L; Kang YJ, An oxygen-releasing device to improve the survival of mesenchymal stem cells in tissue engineering. Biofabrication 2019, 11 (4), 045012. [PubMed: 31315098]
32. Suvarnapathaki S; Wu X; Zhang T; Nguyen MA; Goulopoulos AA; Wu B; Camci-Unal G, Oxygen generating scaffolds regenerate critical size bone defects. Bioactive Materials 2021.
33. Oh SH; Ward CL; Atala A; Yoo JJ; Harrison BS, Oxygen generating scaffolds for enhancing engineered tissue survival. Biomaterials 2009, 30 (5), 757–762. [PubMed: 19019425]
34. Akhavan-Kharazian N; Izadi-Vasafi H, Preparation and characterization of chitosan/gelatin/nanocrystalline cellulose/calcium peroxide films for potential wound dressing applications. Int J Biol Macromol 2019, 133, 881–891. [PubMed: 31028810]
35. Toftdal MS; Taebnia N; Kadumudi FB; Andresen TL; Frogne T; Winkel L; Grunnet LG; Dolatshahi-Pirouz A, Oxygen releasing hydrogels for beta cell assisted therapy. International Journal of Pharmaceutics 2021, 602, 120595. [PubMed: 33892060]
36. de Sousa Araújo E; Stocco TD; de Sousa GF; Afewerki S; Marciano FR; Corat MAF; de Paula MMM; Verde TFCL; Silva MCM; Lobo AO, Oxygen-generating microparticles in chondrocytes-

laden hydrogels by facile and versatile click chemistry strategy. Colloids and Surfaces B: Biointerfaces 2021, 205, 111850. [PubMed: 34015729]

37. Keilin D; Hartree E, On the mechanism of the decomposition of hydrogen peroxide by catalase. Proceedings of the Royal Society of London. Series B-Biological Sciences 1938, 124 (837), 397–405.
38. Lu K-Y; Lin P-Y; Chuang E-Y; Shih C-M; Cheng T-M; Lin T-Y; Sung H-W; Mi F-L, H2O2-depleting and O2-generating selenium nanoparticles for fluorescence imaging and photodynamic treatment of proinflammatory-activated macrophages. ACS applied materials & interfaces 2017, 9 (6), 5158–5172. [PubMed: 28120612]
39. Hu Z; Ding Y, Cerium oxide nanoparticles-mediated cascade catalytic chemo-photo tumor combination therapy. Nano Research 2021, 1–13.
40. Kamiloglu S; Sari G; Ozdal T; Capanoglu E, Guidelines for cell viability assays. Food Frontiers 2020, 1 (3), 332–349.
41. Arunachalam K; Sasidharan SP, Cell Culture Assays. In Bioassays in Experimental and Preclinical Pharmacology, Springer: 2021; pp 3–19.
42. Kumar P; Nagarajan A; Uchil PD, Analysis of cell viability by the lactate dehydrogenase assay. Cold Spring Harbor Protocols 2018, 2018 (6), pdb. prot095497.
43. Pędziwiatr P, Decomposition of hydrogen peroxide-kinetics and review of chosen catalysts. Acta Innovations 2018, (26), 45–52.
44. Wang W; Zhang J; Qiu Z; Cui Z; Li N; Li X; Wang Y; Zhang H; Zhao C, Effects of polyethylene microplastics on cell membranes: A combined study of experiments and molecular dynamics simulations. Journal of Hazardous Materials 2022, 429, 128323. [PubMed: 35086040]
45. McDougal AD; Dewey CF, Modeling oxygen requirements in ischemic cardiomyocytes. Journal of Biological Chemistry 2017, 292 (28), 11760–11776. [PubMed: 28487363]
46. Bon-Mathier A-C; Rignault-Clerc S; Bielmann C; Rosenblatt-Velin N, Oxygen as a key regulator of cardiomyocyte proliferation: New results about cell culture conditions! Biochimica et Biophysica Acta (BBA) - Molecular Cell Research 2020, 1867 (3), 118460. [PubMed: 30885672]
47. AlQathama A; Bader A; Al-Rehaily A; Gibbons S; Prieto JM, In vitro cytotoxic activities of selected Saudi medicinal plants against human malignant melanoma cells (A375) and the isolation of their active principles. European Journal of Integrative Medicine 2021, 102083.
48. Alva R; Mirza M; Baiton A; Lazuran L; Samokysh L; Bobinski A; Cowan C; Jaimon A; Obioru D; Al Makhoul T, Oxygen toxicity: cellular mechanisms in normobaric hyperoxia. Cell Biology and Toxicology 2022, 1–33.
49. Jurisic V; Radenkovic S; Konjevic G, The actual role of LDH as tumor marker, biochemical and clinical aspects. Advances in Cancer Biomarkers 2015, 115–124.
50. Willemen NG; Hassan S; Gurian M; Li J; Allijn IE; Shin SR; Leijten J, Oxygen-Releasing Biomaterials: Current Challenges and Future Applications. Trends in biotechnology 2021.
51. Agarwal T; Kazemi S; Costantini M; Perfeito F; Correia CR; Gaspar V; Montazeri L; De Maria C; Mano JF; Vosough M, Oxygen releasing materials: towards addressing the hypoxia-related issues in tissue engineering. Materials Science and Engineering: C 2021, 111896. [PubMed: 33641899]
52. Boffito M; Sartori S; Ciardelli G, Polymeric scaffolds for cardiac tissue engineering: requirements and fabrication technologies. Polymer International 2014, 63 (1), 2–11.
53. Kargarpoor Z; Nasirzade J; Di Summa F; Panahipour L; Miron RJ; Gruber R, Platelet-Rich Fibrin Can Neutralize Hydrogen Peroxide-Induced Cell Death in Gingival Fibroblasts. Antioxidants 2020, 9 (6), 560. [PubMed: 32604944]
54. Grubecki I; Kazimierska-Drobny K, Prediction of the fixed-bed reactor behavior for biotransformation with parallel enzyme deactivation using dispersion model: A case study on hydrogen peroxide decomposition by commercial catalase. Polish Journal of Chemical Technology 2019, 21 (4), 106–115.
55. Kankala RK; Kuthati Y; Liu C-L; Mou C-Y; Lee C-H, Killing cancer cells by delivering a nanoreactor for inhibition of catalase and catalytically enhancing intracellular levels of ROS. RSC advances 2015, 5 (105), 86072–86081.

Health Research Alliance Author Manuscript

56. Ye G; Metreveli NS; Donthi RV; Xia S; Xu M; Carlson EC; Epstein PN, Catalase protects cardiomyocyte function in models of type 1 and type 2 diabetes. Diabetes 2004, 53 (5), 1336–1343. [PubMed: 15111504]

57. Elmsmari F; González Sánchez JA; Duran-Sindreu F; Belkadi R; Espina M; García ML; Sánchez-López E, Calcium hydroxide-loaded PLGA biodegradable nanoparticles as an intracanal medicament. International Endodontic Journal 2021, 54 (11), 2086–2098. [PubMed: 34355406]

58. Cerda-Cristerna BI; Breceda-Leija A; Méndez-González V; Chavarría-Bolaños D; Flores-Reyes H; Garrocho-Rangel A; Komabayashi T; Wadajkar AS; Pozos-Guillén AJ, Sustained release of calcium hydroxide from poly (dl-lactide-co-glycolide) acid microspheres for apexification. Odontology 2016, 104 (3), 318–323. [PubMed: 26175086]

59. Accorinte M. d. L. R.; Holland R; Reis A; Bortoluzzi MC; Murata SS; Dezan E; Souza V; Alessandro LD, Evaluation of Mineral Trioxide Aggregate and Calcium Hydroxide Cement as Pulp-capping Agents in Human Teeth. Journal of Endodontics 2008, 34 (1), 1–6. [PubMed: 18155482]

60. Wu C-S; Wu D-Y; Wang S-S, Antibacterial properties of biobased polyester composites achieved through modification with a thermally treated waste scallop shell. ACS Applied Bio Materials 2019, 2 (5), 2262–2270.

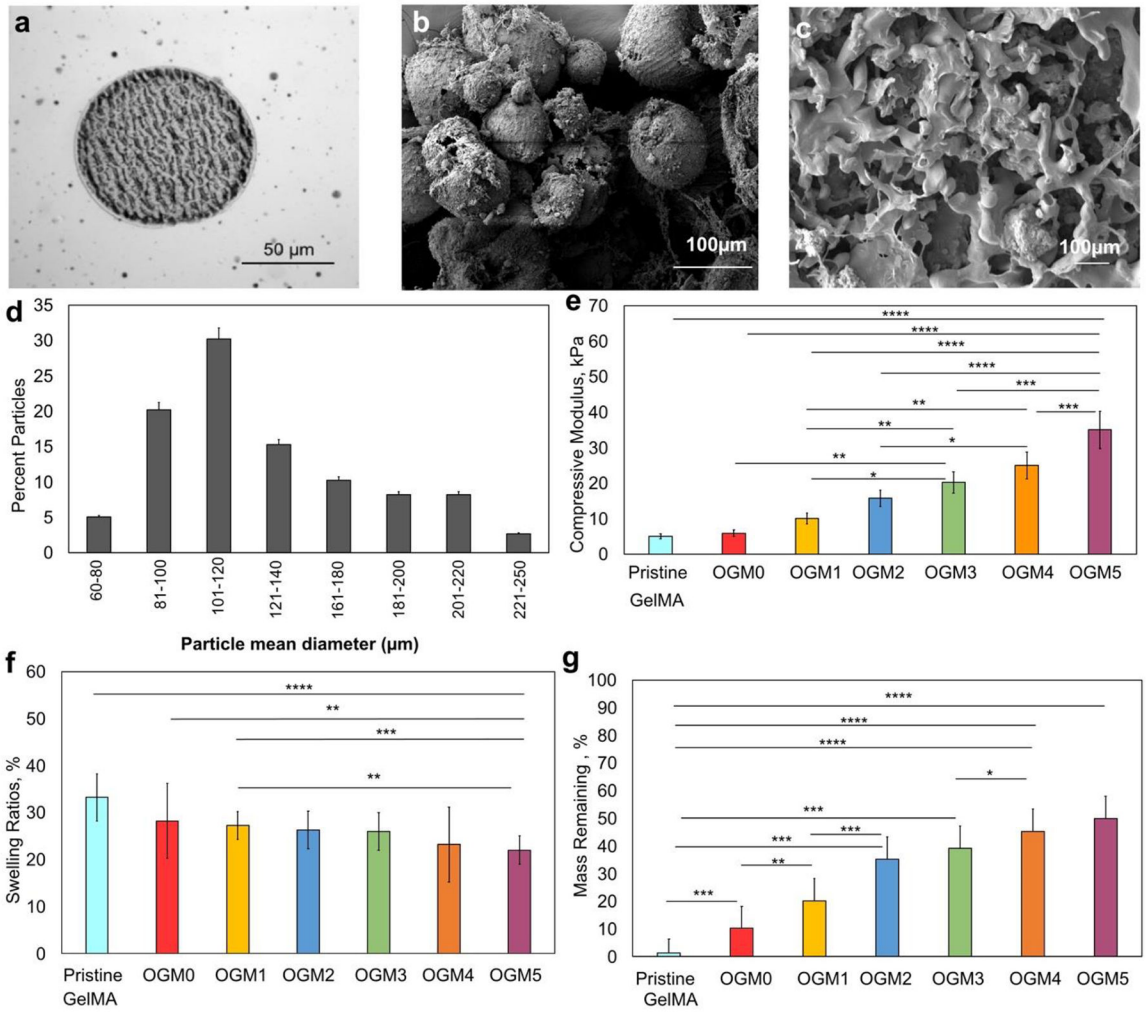

Figure 1.

Characterization of the physical properties of the oxygen-generating microspheres. a. Phase contrast imaging, b. SEM analysis c. SEM imaging to demonstrate the microparticles within the hydrogel matrix, d. Analysis of average particle diameter and size distribution, e. DMA compression test, f. Swelling and g. Degradation analyses. The assessment of the physical properties revealed correlations between different scaffold compositions. Particularly the CaO_2 concentrations within PCL and their tunable effects on the material properties of the resulting composite scaffolds were evaluated. The results showed that with an increase in the CaO_2 concentration within PCL, the swelling ratios of the composite scaffold decreased, the degradation rate decreased, and the mechanical strength of the scaffolds increased, as expected.

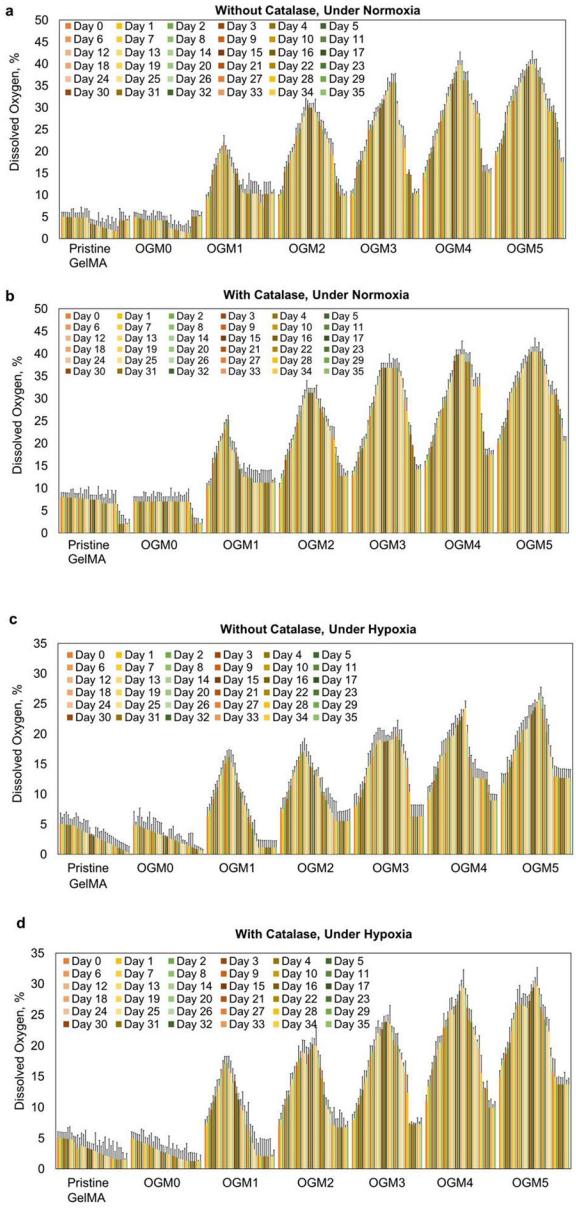

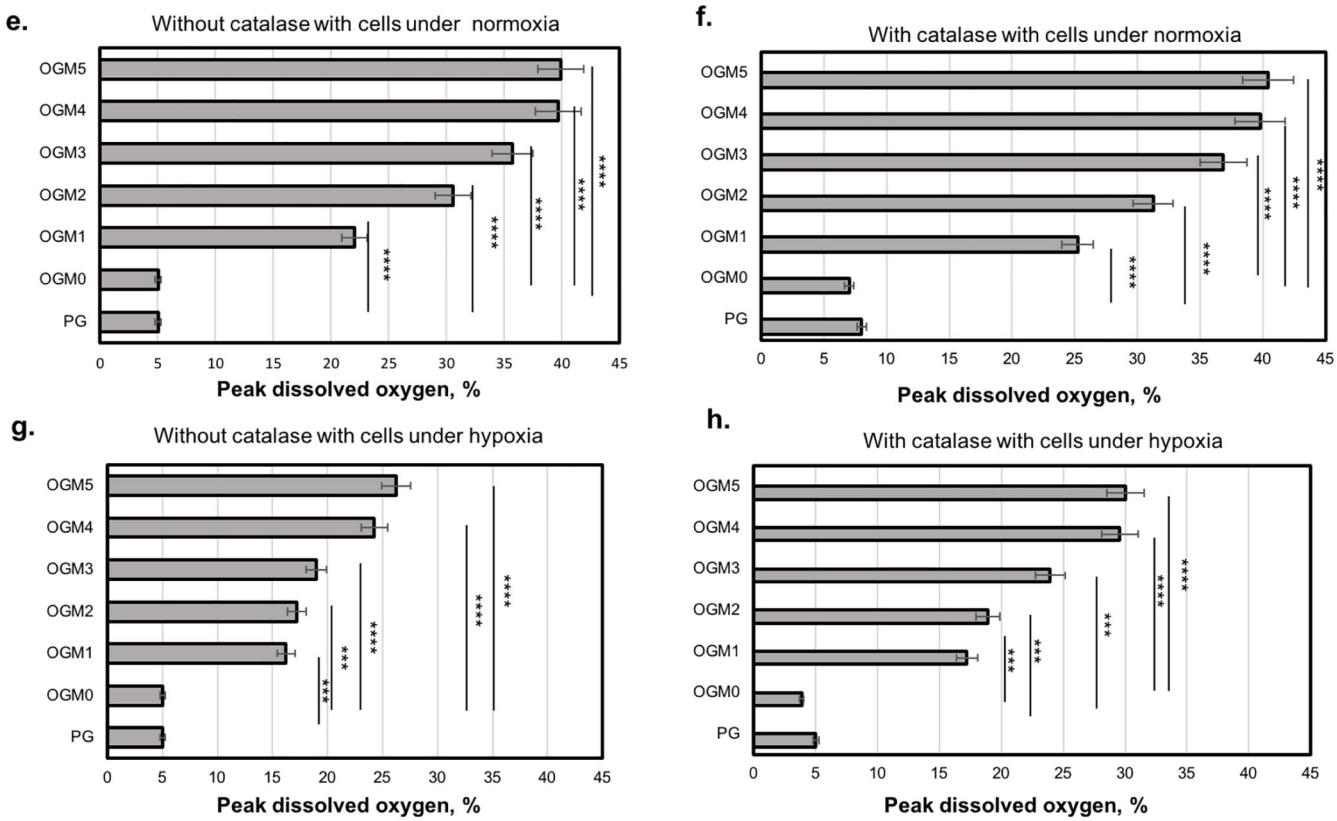

Figure 2.

Oxygen release kinetics of different scaffold compositions with microencapsulated H9c2 cardiomyocytes evaluated using the NeoFox oxygen sensing probe a. Without catalase under normoxia, b. With catalase under normoxia, c. Without catalase under the hypoxic condition, and d. With 1 mg/mL catalase under induced hypoxia. The oxygen probe measured the partial pressure of oxygen within the supernatant media used to culture these scaffolds, which is read out proportionally as percent dissolved oxygen. The dissolved oxygen levels in the supernatant increased in proportion to the CaO_2 concentration within the scaffolds. The OGM4 and OGM5 scaffolds thereby showed the highest peak percentage dissolved oxygen levels and highest dissolved oxygen percent by Day 35 compared to the pristine GelMA, OGM0, OGM1, OGM2 and OGM3 groups. The peak % dissolved oxygen levels were compared for each scaffold composition when cultured e. Without catalase with cells under normoxia, f. With catalase with cells under normoxia, g. Without catalase with cells under hypoxia, and h. With catalase with cells under hypoxia.

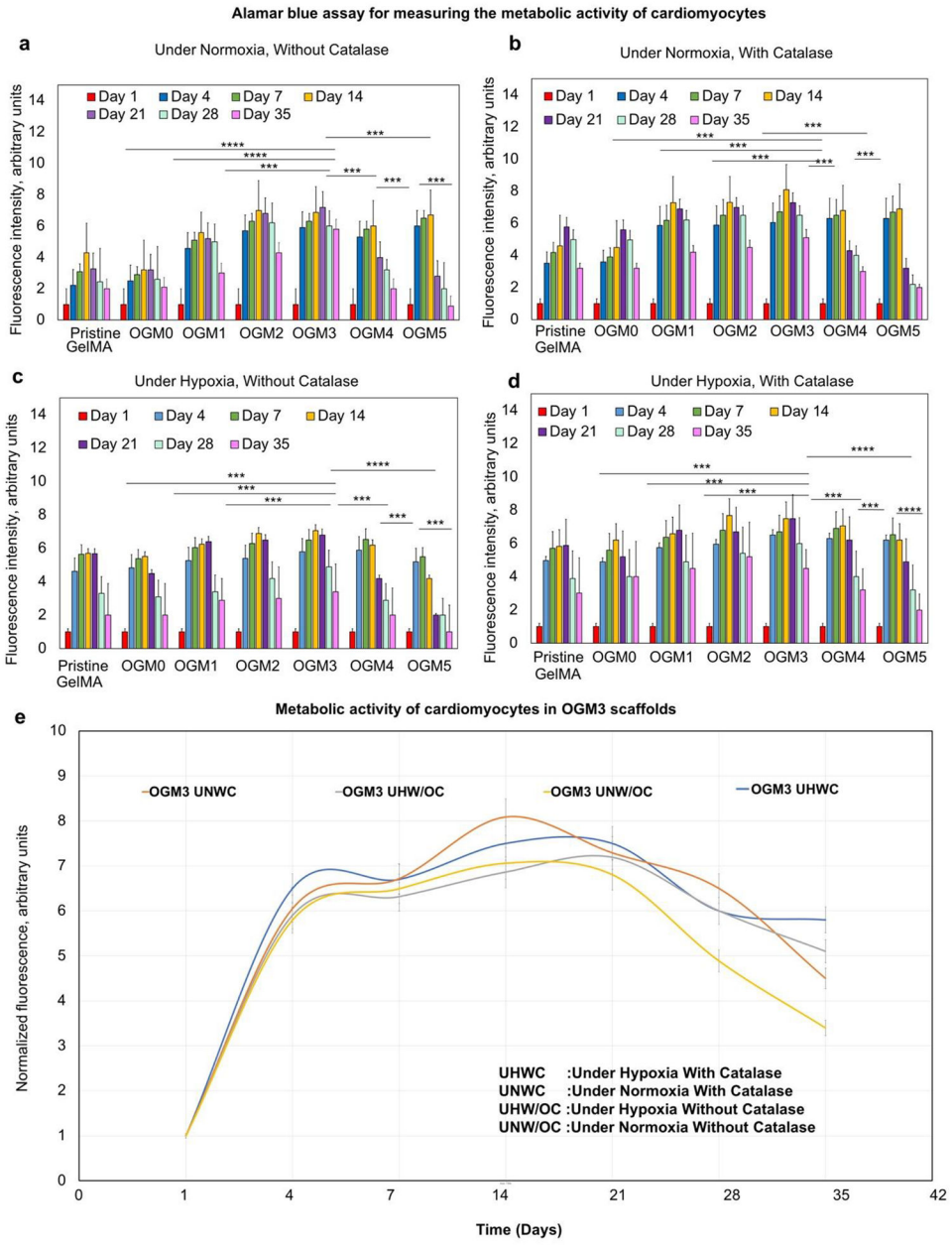

Figure 3.

Cellular metabolic activity of encapsulated H9c2 cardiomyocytes evaluated using Alamar Blue assay a. Under normoxia without catalase, b. Under normoxia with catalase, c. Under hypoxia without catalase, and d. Under hypoxia with catalase; e. The OGM3 scaffolds displayed the highest metabolic activity over 35 days across all culture conditions. The comparative analysis of the metabolic activity within the OGM3 scaffolds was performed under all culture conditions. The OGM4 and OGM5 scaffolds caused a decline in the cellular metabolic activity despite their high oxygen content, indicating excessive oxygen concentrations decrease the cellular metabolic activity.

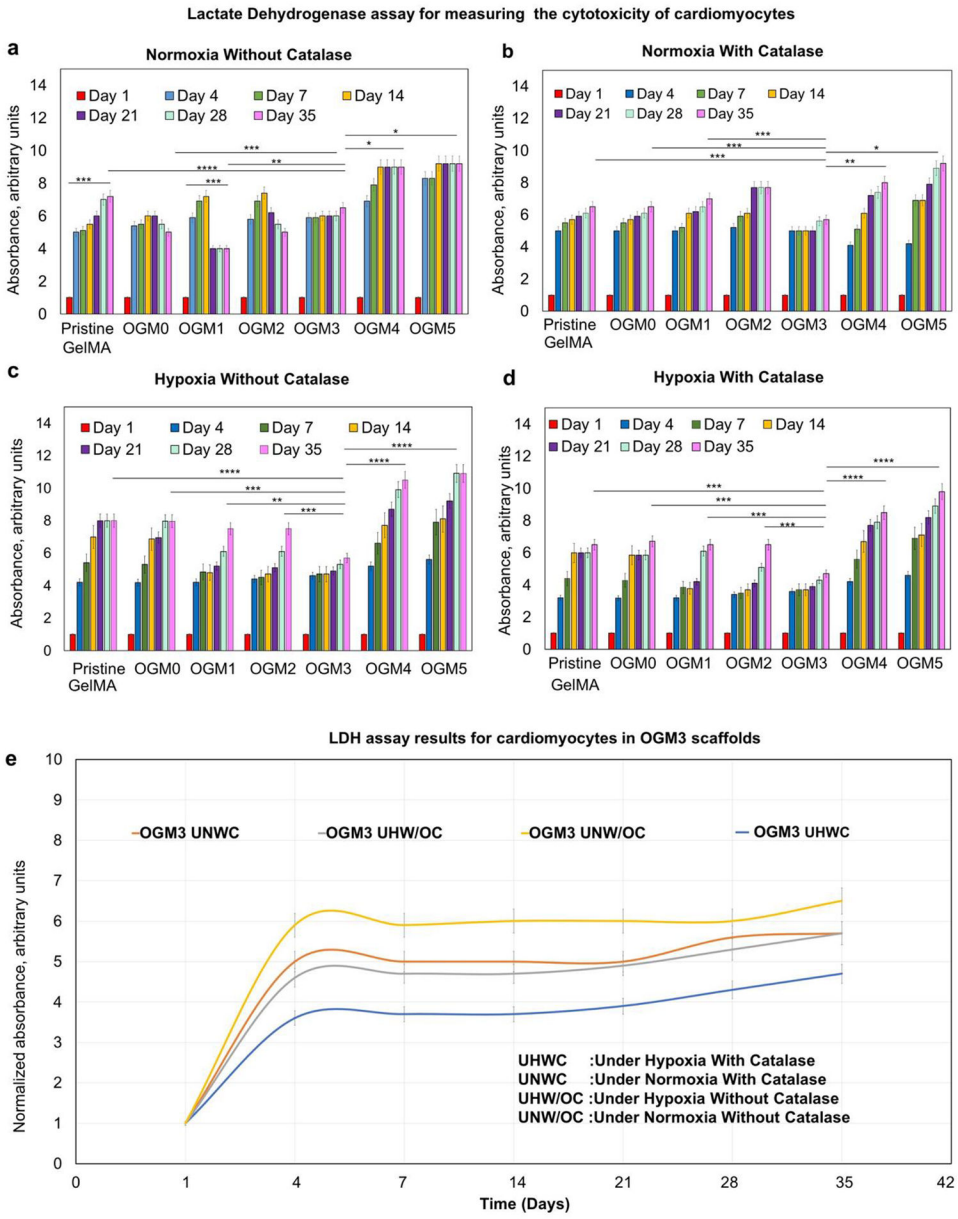

Figure 4.

Cytotoxicity evaluation for the oxygen-generating scaffolds using lactate dehydrogenase (LDH) assay for the samples that were cultured a. Under normoxia without catalase, b. Under normoxia with catalase, c. Under hypoxia without catalase, and d. Under hypoxia with catalase. E. The comparative LDH activity analyses within the OGM3 scaffolds under all culture conditions showed no increase in the LDH levels over the 35-day culture period. The OGM3 scaffolds therefore indicated no cytotoxicity whereas the pristine GelMA, OGM0, OGM4, and OGM5 scaffolds showed an increasing LDH levels in comparison. The OGM3 scaffolds demonstrated the most favorable cellular response and did not elicit cytotoxicity under all of the culture conditions.

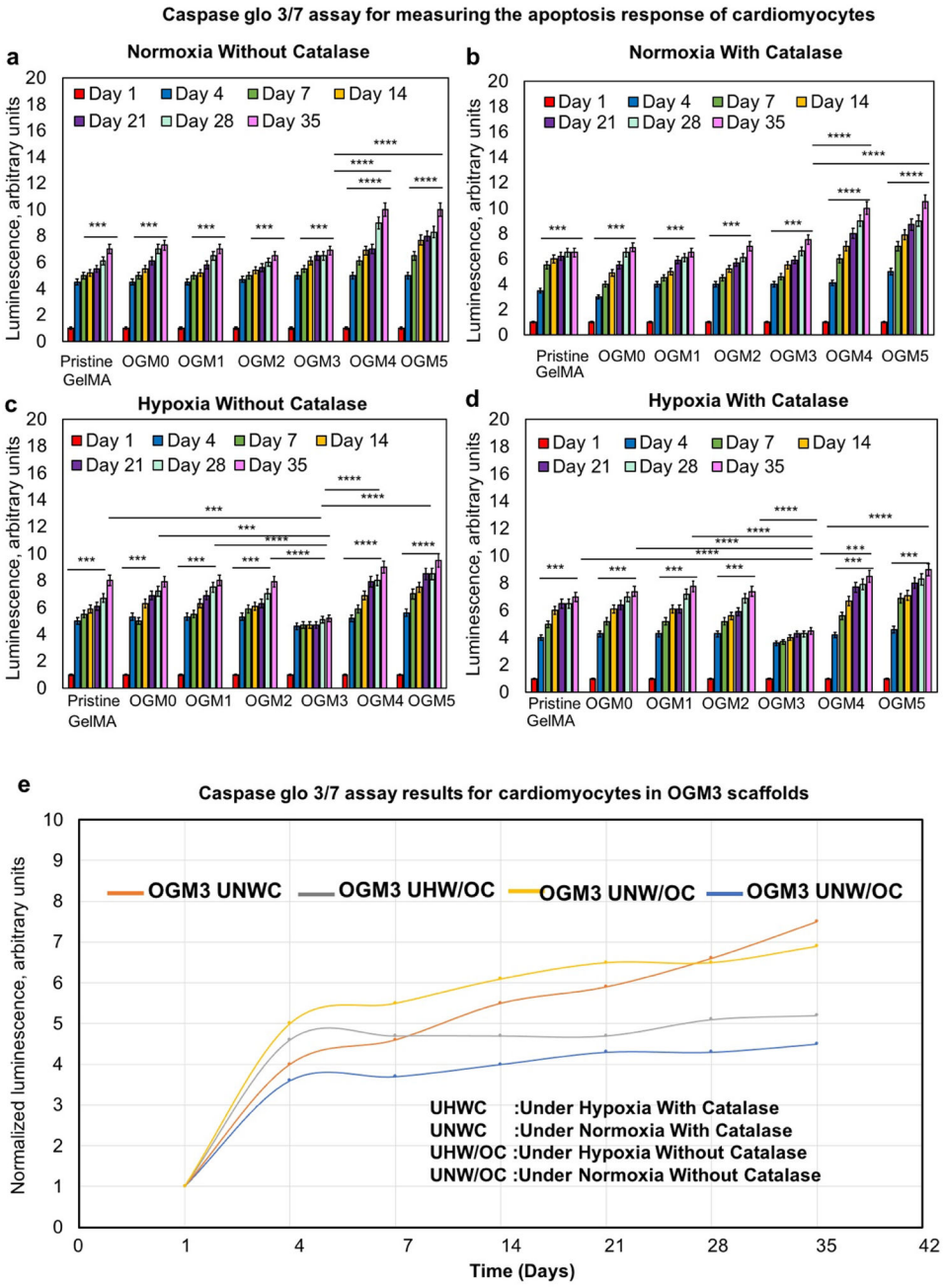

Figure 5.

Apoptosis response to oxygen-generating scaffolds was evaluated using the Caspase Glo 3/7 assay a. Under normoxia without catalase, b. Under normoxia with catalase, c. Under hypoxia without catalase, and d. Under hypoxia with catalase. The comparative normalized luminescence is shown in e. The OGM3 scaffolds showed no significant increase in the caspase activity over 35 days under all culture conditions. The pristine GelMA, OGM0, OGM1, OGM2, OGM4, and OGM5 scaffolds revealed a gradual increase in the caspase activity compared to the OGM3 scaffolds. The OGM3 scaffolds demonstrated the most

favorable cellular response and did not elicit increasing apoptosis within the encapsulated cardiomyocytes.

Health Research Alliance Author Manuscript

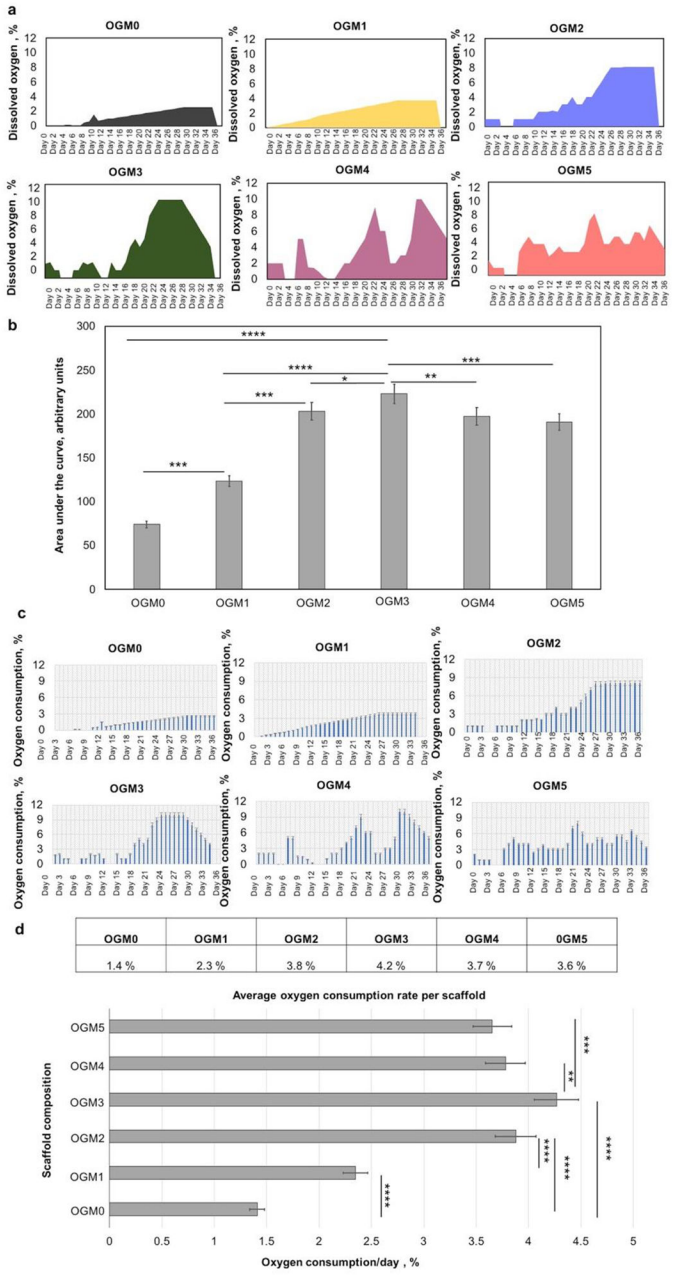

Figure 6.

Evaluation of the net oxygen consumption and the oxygen consumption rates of the encapsulated H9c2 cardiomyocytes within the oxygen-generating scaffolds. A. The net oxygen consumption within each scaffold composition was monitored and recorded over 35 days, b. The area under the curve for each scaffold was quantified and compared. The OGM3 scaffolds had a significantly higher net oxygen consumption compared to the other scaffold groups. C. The oxygen consumption rate per day was calculated. The OGM3 scaffolds exhibited the fastest oxygen consumption rate over 35 days. The quantification of

the oxygen release capacity and net oxygen consumption revealed a positive correlation with cellular response. The OGM3 scaffolds presented optimized cellular response.

Health Research Alliance Author Manuscript

Health Research Alliance Author Manuscript

Table 1.

Nomenclature for the oxygen-generating scaffolds that were synthesized in 13.5% w/v PCL and encapsulated in 5% w/v GelMA.

Scaffold nomenclature	Calcium peroxide (mg/mL) in PCL	Calcium peroxide (mg/mL) in GelMA
OGM0	0	0
OGM1	20	2.7
OGM2	40	5.4
OGM3	60	8.1
OGM4	80	10.8
OGM5	100	13.5